

Mapping key soil micronutrients across the Tibetan Plateau ~~Mapping soil trace elements (Fe Mn Zn Ni) on the Tibetan Plateau~~

Huangyu Huo^{1,2}, Xiling Gu^{1,2}, Jiayi Li^{1,2}, Shanshan Yang¹, Yafeng Wang^{1*}, Jinzhi Ding^{1*}

¹State Key Laboratory of Tibetan Plateau Earth System, Environment and Resources (TPESER), Institute of Tibetan Plateau Research, Chinese Academy of Sciences, Beijing 100101, China.

²University of Chinese Academy of Sciences, College of Resources and Environment, Beijing 100049, China.

*Corresponding to: Jinzhi Ding (jzding@itpcas.ac.cn), Yafeng Wang (yfwang@itpcas.ac.cn)

Abstract. Soil micronutrients supply sustains critical ecological functions but exhibit poorly quantified distribution patterns in high-altitude ecosystems. This study bridges this knowledge gap through a large-scale investigation across the Tibetan Plateau, a cold-arid region where cryogenic weathering, aridity, and suppressed pedogenesis interact to govern micronutrient cycling. We assembled a plateau-wide dataset from 526 sites with triplicate surface soils (0-10 cm) per site (n = 1,660). Seven micronutrients (Fe, Mn, Cu, Zn, Ni, V, Mo) were measured and paired with multi-source predictors (climate, vegetation, soil properties, topography, graze disturbance, and weathering proxy). Elemental contents span broad ranges, with site-level summaries (mean \pm SD, mg \cdot kg⁻¹) of Fe 22,864.30 \pm 7,589.01, Mn 576.74 \pm 206.44, Cu 25.32 \pm 9.28, Zn 27.24 \pm 8.55, Ni 49.35 \pm 10.98, V 56.99 \pm 19.33, and Mo 4.63 \pm 1.14. Random Forest model was employed to quantify controls and generate high-resolution spatial maps. Key results reveal that pronounced regional heterogeneity driven primarily by climate-related weathering intensity and topography variable, with secondary modulation from soil and vegetation factors. Element-specific spatial patterns were observed, with Fe enrichment in southeastern/southern plateaus, Mn gradients increasing southeastward and Cu over the western-northern plateau with minima in the southeast. Zn hotspots in central-eastern and western marginal zones, Ni enriched across the northern-central interior and western highlands, and V exhibits a moderate spatial gradient, with higher contents in the southeastern Tibetan Plateau and relatively lower values in the northwest. Mo weakly patterned, slightly higher on northern basins and lower toward the southeast. We provide 1-km maps of all seven micronutrients together with pixel-wise uncertainty layers to support benchmarking of process-based micronutrient cycling models and to inform sustainable ecosystem management under climate change. The dataset is openly available at TPDC (<https://doi.org/10.11888/Terre.tpdc.303049>; Huo et al., 2025).

~~Soil Micronutrients supply sustain critical ecological functions but exhibit poorly quantified distribution patterns in high-altitude ecosystems. This study bridges this knowledge gap through a large-scale investigation across the Tibetan Plateau, a cold-arid region where cryogenic weathering, aridity, and suppressed pedogenesis interact to govern microelement cycling. We selected 526 spatially representative sites spanning climatic and edaphic gradients, analyzing six microelements (Fe, Mn,~~

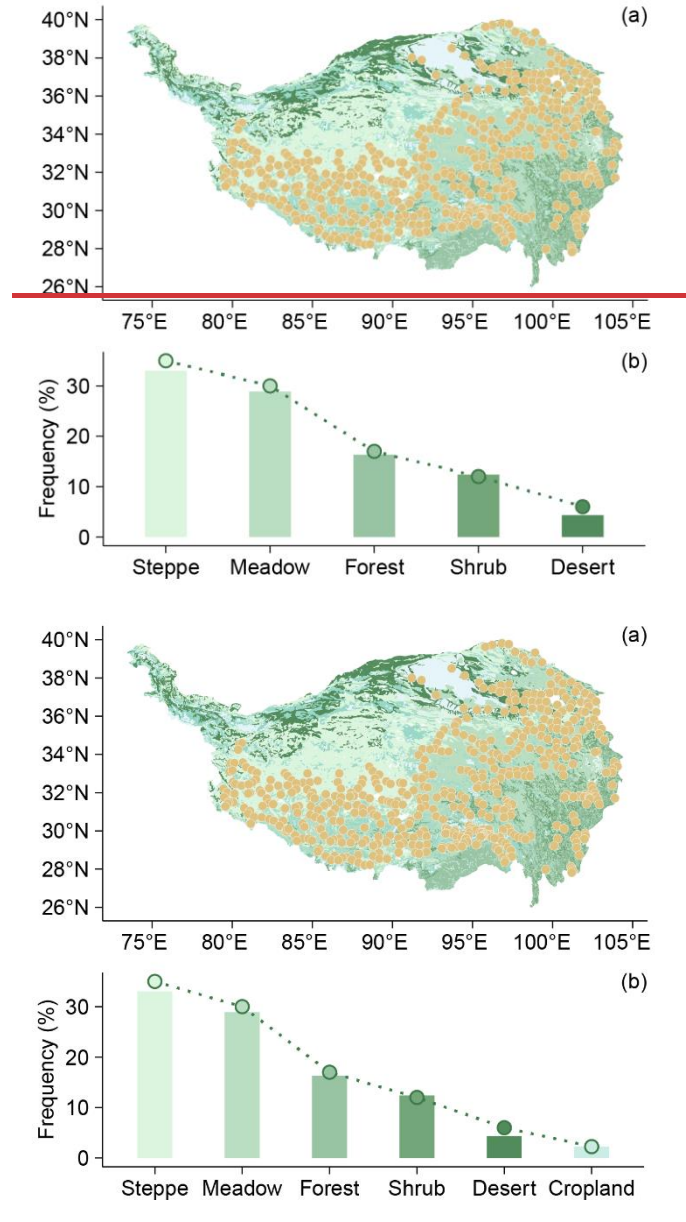
30 ~~Zn, Ni, Cu, Mo) alongside multi factorial drivers (climate, vegetation, soil, topography, human disturbances, weathering~~
31 ~~proxies). Random Forest modeling was employed to quantify controls and generate high resolution spatial maps. Key results~~
32 ~~reveal that pronounced regional heterogeneity driven primarily by moisture related climatic variables (mean annual~~
33 ~~precipitation, aridity index), with secondary modulation from weathering intensity and vegetation factors. Element specific~~
34 ~~spatial patterns were observed, with Fe enrichment in southeastern/southern plateaus, Mn gradients increasing southwestward~~
35 ~~and Zn hotspots in central eastern and western marginal zones. The machine learning derived maps with a 1 km resolution~~
36 ~~serve for benchmarking process based microelement cycling models and rooting for sustainable ecosystem management~~
37 ~~under climate change.~~

38 1 Introduction

39 As essential yet trace-level components of living systems, micronutrients (e.g., Fe, Mn, Cu, Zn, Ni, [V](#), Mo) sustain
40 fundamental ecological processes, including photosynthesis (Fe, Mn; Fischer et al., 2015; Schmidt et al., 2020), respiration
41 (Fe; Dallman, 1986), enzymatic/redox functions (Cu, Zn, Mn, [V](#); Hänsch et al., 2009), and biological nitrogen fixation (Ni, [V](#),
42 Mo; O'Hara, 2001). Crucially, micronutrient gradients in soils propagate through trophic chains, directly influencing human
43 nutrition and health; deficiencies exacerbate global malnutrition burdens (Fageria et al., 2002; White et al., 2005). Despite
44 their pivotal role in ecosystem stability and food security (Presteele et al., 2016; Stehfest et al., 2019), critical knowledge
45 gaps persist regarding the distribution patterns and drivers of soil micronutrients from regional to global scales.

46 Soil micronutrient supply originates from coupled physicochemical weathering and biological mediation, critically regulated
47 by local climate and topography (Ochoa-Hueso et al., 2020; Hartmann et al., 2023). In cold-arid high-altitude regions,
48 particularly the Tibetan Plateau, extreme environmental interactions uniquely govern micronutrient cycling. Cryogenic
49 processes such as glacial erosion and freeze-thaw cycles, accelerate physical bedrock weathering to mobilize lithogenic
50 micronutrient reservoirs, while aridity concurrently constrains chemical weathering and elemental release (Mu et al., 2020;
51 Mu et al., 2016). Low temperatures suppress biological turnover and synergize with aridity to compromise pedogenesis
52 through clay deficits and diminished mineral reactive sites, thereby reducing elemental retention capacity (Dijkstra et al.,
53 2004). These counteracting processes fundamentally shape [micronutrientsmicroelements](#)—distribution patterns, yet remain
54 severely understudied. Current research is largely restricted to localized transects (e.g., Heihe River Basin, Tibetan Plateau
55 Highway) with limited spatial representation ([Zhang et al., 2012](#); [Guan et al., 2017](#); [Bu et al., 2016](#)).

56 To address these knowledge gaps, we conducted a large-scale field investigation across the Tibetan Plateau, establishing 526
57 sampling sites distributed across representative temperature and moisture gradients (Fig. 1). The sampling design
58 encompassed the plateau's dominant vegetation types and lithological classes. Using this dataset, we analyzed distribution
59 patterns and key controlling factors for ~~sevensix~~ essential trace elements (Fe, Mn, Cu, Zn, Ni, [V](#), Mo_s). We then applied a
60 Random Forest algorithm to generate high-resolution spatial distribution maps of these [micronutrientsmicroelements](#),
61 representing the first comprehensive quantification at this scale and resolution.



62

63

64 **Figure 1.** Sampling strategy and ecosystem representativeness. (a) Spatial distribution of sampling sites superimposed on China's
 65 1:1,000,000 vegetation map. (b) Areal proportions of ecosystem types (bars) versus sampling point frequency distribution (dots) across
 66 corresponding ecosystems. Similar bar and dot heights indicate that the sampling is proportionally representative.

67 **2 Methods**

68 **2.1 Field survey and soil micronutrients~~microelements~~ analysis**

69 We analyzed 1,660 topsoil samples collected from 526 locations during a 2019-2021 growing season (July-August) field
 70 survey across the Tibetan Plateau (79-105°E, 27-40°N; Fig. 1a). Sampling sites represent major plateau ecosystems: forests,
 71 shrubs, steppes, meadows, deserts, and croplands~~deserts~~ (Table 1). The sites span broad environmental gradients, ranging
 72 from 759 to 5565 m in elevation, -7.83 to 18.46 °C in mean annual temperature (MAT), and 23 to 898 mm in mean annual

73 precipitation (MAP), effectively capturing the plateau's topographic and climatic variability. Site was selected using
74 standardized criteria: maintaining relative homogeneity in species composition, community structure, and habitat conditions,
75 and avoiding proximity to roads or areas with frequent human activity. At each location, we established a 15_m_-transect
76 collecting triplicate soil samples (0-10 cm depth) at 0 m, 7.5 m, and 15 m positions. This depth was chosen because it
77 represents the biologically active surface horizon most relevant to plant uptake and microbially mediated cycling, and is
78 widely used in regional soil inventories for comparability across ecosystems. On the Tibetan Plateau, steppes and meadows
79 constitute the dominant land cover, so most samples correspond to mineral A horizons; in forested sites, the 0-10 cm layer
80 may include an organic-rich surface. This consistent protocol ensures cross-site comparability while capturing the variability
81 of surface layer that most strongly interacts with vegetation and climate. Geographic coordinates, elevation, community type,
82 and species composition (Cheng et al., 2022) were systematically documented.

83 To ensure the reliability of soil micronutrient measurements, we adopted a two-step analytical strategy. First, in situ
84 measurements were conducted using a second-generation portable Niton X-ray fluorescence (XRF) analyzer to obtain
85 preliminary contents under natural field conditions. However, because this instrument could not reliably detect Mo, all soil
86 samples were subsequently air-dried, sieved (2 mm), and re-analyzed in the laboratory using a third-generation XRF.
87 Compared with the second-generation device, the third-generation XRF offers an extended detection range and improved
88 accuracy (Lemière, 2018). All data presented in this study are based on the laboratory XRF measurements.

89 To further validate the laboratory XRF results, a subset of 218 samples was randomly selected and re-analyzed using
90 Inductively coupled plasma-Mass Spectrometry (ICP-MS), a widely accepted reference method (Simon, 2005). The two
91 methods showed strong correlations for Fe, Mn, Cu and V ($R^2 = 0.67-0.89$, $P < 0.001$), with values closely aligning with the
92 1:1 line, indicating reliable quantification. For Zn and Ni, XRF and ICP-MS results were also significantly correlated,
93 though systematic deviations from the 1:1 line were observed (Fig. S1). XRF tended to slightly over- or underestimated
94 absolute contents of Zn and Ni contents compared with ICP-MS. To address this, we calibrated Zn and Ni, using the
95 regression relationships between the two methods and then repeated spatial mapping. For Mo, the results obtained from the
96 two methods were not fully consistent, likely due to its low content. Comparative results of both methods are provided in the
97 Supplementary Information (Figs. S2-S4).

98 ~~The portable Niton X ray fluorescence (XRF) spectrometer was deployed in the field to determine total soil concentrations~~
99 ~~of Fe, Mn, Cu, Zn, Ni, and Mo, leveraging its portability and compact design. Reference background values (Lindsay 1979)~~
100 ~~include Fe: 3.8×10^4 mg kg⁻¹, Mn: 6.0×10^2 mg kg⁻¹, Cu: 30 mg kg⁻¹, Zn: 50 mg kg⁻¹, Ni: 40 mg kg⁻¹, and Mo: 1.7 mg kg⁻¹.~~
101 ~~The contents of trace elements, including arsenic (As), barium (Ba), cadmium (Cd), cobalt (Co), chromium (Cr), lead (Pb),~~
102 ~~strontium (Sr), and titanium (Ti), were determined using XRF spectroscopy. Powdered samples were pressed into pellets and~~

analyzed with a wavelength dispersive XRF spectrometer. The instrument was calibrated using certified reference materials to ensure analytical accuracy and comparability.

Table 1. Ecosystem classification and sampling coverage on the Tibetan Plateau, with vegetation traits and sampling intensity.

<u>Biome</u>	<u>Characteristics and dominant plant species</u>	<u>elevation ranges</u>	<u>climate conditions (temperature/precipitation)</u>	<u>No. of samples</u>	<u>No. of locations</u>
<u>Steppe</u>	<u>Alpine steppes, dominated by cold-adapted herbaceous species such as <i>Stipa purpurea</i>, features sparse vegetation adapted to cold-arid conditions.</u>	<u>1961-5151 m</u>	<u>-7.1-8.0 °C; 34.32-785.61 mm</u>	<u>569</u>	<u>180</u>
<u>Meadow</u>	<u>Alpine meadows feature dense, low-stature vegetation sustained by year-round low temperatures, high humidity, and water-retentive soils. These ecosystems thrive on gentle slopes and valley floors at higher elevations, hosting relatively diverse flora with characteristic dominance of sedges including <i>Kobresia pygmaea</i> and <i>K. humilis</i>.</u>	<u>2661-5565 m</u>	<u>-7.8-9.2 °C; 158.42-848.70 mm</u>	<u>499</u>	<u>154</u>
<u>Forest</u>	<u>Forests on the Tibetan Plateau concentrate primarily in the southeastern region, dominated by high-altitude cold-temperate coniferous forests. These humid-adapted ecosystems feature <i>fir (Abies)</i> and <i>spruce (Picea)</i> species as characteristic components.</u>	<u>1453-4237 m</u>	<u>-0.6-16.5 °C; 400.34-898.48 mm</u>	<u>265</u>	<u>87</u>
<u>Shrub</u>	<u>Tibetan shrublands primarily occur in arid and alpine zones, characterized by low-growing, drought-tolerant dwarf shrubs such as <i>Lonicera (honeysuckle)</i> and <i>Rhododendron</i> species adapted to nutrient-poor soils and extreme climatic conditions.</u>	<u>2169-5022 m</u>	<u>-5.2-11.8 °C; 301.40-868.63 mm</u>	<u>190</u>	<u>64</u>
<u>Desert</u>	<u>Alpine deserts occur in extremely arid, cold regions and exhibit extremely sparse vegetation dominated by <i>arid-tolerant dwarf shrubs</i> and <i>herbs</i>.</u>	<u>2108-5158 m</u>	<u>-7.1-5.6 °C; 22.64-443.43 mm</u>	<u>101</u>	<u>29</u>
<u>Cropland</u>	<u>Cropland, concentrated in river valleys and basin floors and is dominated by highland barley (<i>Hordeum vulgare</i> var. <i>nudum</i>, “qingke”), with spring wheat (<i>Triticum aestivum</i>), rapeseed (<i>Brassica napus</i>), and potato (<i>Solanum tuberosum</i>) commonly cultivated; vegetation cover is strongly seasonal and often bare after harvest.</u>	<u>759-4360 m</u>	<u>0.5-18.4 °C; 112.53-783.06 mm</u>	<u>36</u>	<u>12</u>

<u>Biome</u>	<u>Characteristics</u>	<u>No. of samples</u>	<u>No. of locations</u>
<u>Steppe</u>	<u>Alpine steppes, dominated by cold-adapted herbaceous species such as <i>Stipa purpurea</i>, features sparse vegetation adapted to cold-arid conditions.</u>	<u>578</u>	<u>183</u>
<u>Meadow</u>	<u>Alpine meadows feature dense, low-stature vegetation sustained by year-round low temperatures, high humidity, and water-retentive soils. These ecosystems thrive on gentle slopes and valley floors at higher elevations, hosting relatively diverse flora with characteristic dominance of sedges including <i>Kobresia pygmaea</i> and <i>K. humilis</i>.</u>	<u>505</u>	<u>156</u>

Forest	Forests on the Tibetan Plateau concentrate primarily in the southeastern region, dominated by high altitude cold-temperate coniferous forests. These humid-adapted ecosystems feature fir (<i>Abies</i>) and spruce (<i>Picea</i>) species as characteristic components.	280	92
Shrub	Tibetan shrublands primarily occur in arid and alpine zones, characterized by low-growing, drought-tolerant dwarf shrubs such as <i>Lonicera</i> (honeysuckle) and <i>Rhododendron</i> species adapted to nutrient-poor soils and extreme climatic conditions.	193	65
Desert	Alpine deserts occur in extremely arid, cold regions and exhibit extremely sparse vegetation dominated by arid-tolerant dwarf shrubs and herbs.	104	30

Biomes are grouped by diagnostic characteristics; dominant plant species are italicized. Elevation range gives the minimum-maximum elevation (m) of sampling sites within each biome. Climate conditions report site-level ranges of mean annual temperature (°C) and mean annual precipitation (mm). No. of samples is the number of soil samples analyzed (0-10 cm, three replicates per site), and No. of locations is the number of unique sampling sites.

2.2 Soil Properties

Soil samples were sifted through 2 mm sieve, discarding visible stones and extracted roots. Soil pH was measured using the potentiometric method, and soil texture analysis, quantifying clay, silt, and sand content fractions, was determined using a laser diffraction particle size analyzer (Mastersizer 2000, Malvern, UK). The sieved samples were air-dried for elemental analysis. Soil organic carbon (SOC) content was quantified via the potassium dichromate oxidation method (Walkley-Black) with external heating. ~~Total carbon (C) and total nitrogen (N) contents were measured using a Vario EL III elemental analyzer (Elementar, Germany). Total phosphorus (P) was extracted with sodium bicarbonate (Olsen method) and determined by molybdenum-antimony anti-spectrophotometry. The concentrations of sulfur (S), potassium (K), calcium (Ca), sodium (Na), magnesium (Mg), and aluminum (Al) were determined using XRF spectroscopy.~~ The chemical index of alteration (CIA) was calculated using the molar proportions of Al_2O_3 , CaO^* , Na_2O , and K_2O according to the formula: $CIA = Al_2O_3 / (Al_2O_3 + CaO^* + Na_2O + K_2O)$. ~~All oxide concentrations were determined by X-ray fluorescence spectroscopy and converted to molar units. CaO^* represents CaO derived solely from silicate minerals, with carbonate contributions excluded where applicable.~~ $\times 100$ (Fedo et al., 1995). The chemical index of alteration reflects the relative loss of mobile base cations (Ca, Na, K) compared with the enrichment of immobile Al during weathering (McLennan, 1993). Higher chemical index of alteration values indicate stronger chemical weathering and more advanced soil development, whereas lower values suggest weaker weathering and limited leaching of base cations (Nesbitt et al., 1982).

2.3 Environmental variables

127 We considered geographic, climatic, biological, and edaphic drivers. Field measurements provided location (longitude,
128 latitude), slope, aspect and vegetation type. For the spatial prediction of micronutrient distributions, however, the gridded
129 predictor variables (e.g., elevation, slope, aspect, vegetation cover) were derived from online datasets in order to upscale
130 site-level observations to the Plateau scale. while sSlope and aspect data came from the National Tibetan Plateau Data Center
131 (<https://data.tpd.ac.cn>). The digital elevation model (DEM) data were collected from the Resource and Environment
132 Science and Data Center (<https://www.resdc.cn/>). Climate variables, mean annual temperature (MAT) and mean annual
133 precipitation (MAP) were downloaded from the Climate Data Store (<https://cds.climate.copernicus.eu#!/home>). The Aridity
134 Index (AI), calculated as mean annual precipitation/mean annual reference evapotranspiration, was obtained from the Global
135 Aridity Index dataset (Trabucco et al., 2018), where higher values indicate greater humidity. Vegetation types (Forest, Shrub,
136 Meadow, Steppe, Desert, Cropland) followed the 1:1,000,000 China Vegetation Map classification (Hou, 2019). The
137 normalized difference vegetation index (NDVI) data were obtained from an Earthdata Search (<https://search.earthdata.nasa.gov/search>). The net primary productivity (NPP) data were obtained from the study by Chen et al. (2023) and
138 were calculated using the CASA model (Potter et al., 1993). The grazing activity data were obtained from statistical
139 yearbooks. Based on the lithological data published by Dijkshoorn et al. in 2018, the rock types on the Tibetan Plateau were
140 classified into acidic igneous rock (IA), acidic metamorphic rock (MA), clastic sedimentary rock (SC), carbonate rock (SO),
141 aeolian facies rock (UE), and fluvial facies rock (UF).

143 **2.4 Relative importance analysis and soil micronutrient mapping**

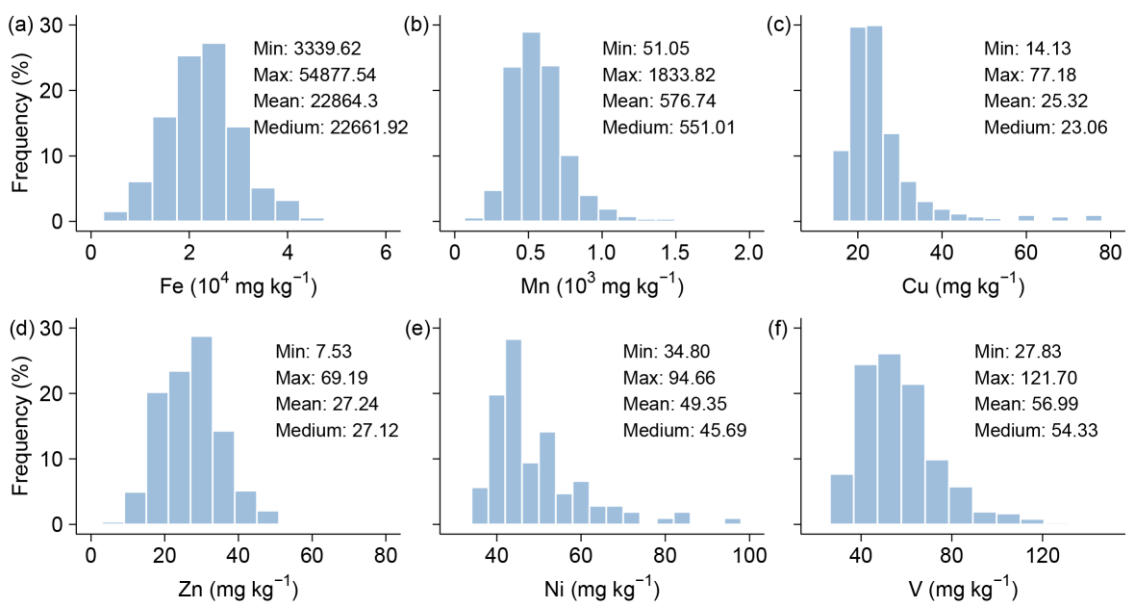
144 Soil ~~micronutrient~~microelement measurements were preprocessed to detect and remove outliers exceeding the mean \pm 3
145 standard deviations. After data screening, the retained sample sizes are: Fe 1654 (from 1660), Mn 1630 (from 1646), Cu 920
146 (from 946), Zn 1655 (from 1661), Ni 180 (from 181), V 857 (from 867), and Mo 120 (from 123). To evaluate the relative
147 importance of predictors in explaining soil micronutrient variability across the Tibetan Plateau, we applied the random forest
148 permutation importance (%IncMSE) to independently cross-validate the driver rankings. we applied the ‘betasq’ metric from
149 the calc.relimp function in the R package relaimpo (Grömping, 2006), which is based on squared standardized regression
150 coefficients and accounts for differences in variable scales and units. For spatial prediction, we developed ~~sevensix~~seven area-wide
151 random forest models (each comprising 500 trees) targeting Fe, Mn, Cu, Zn, Ni, V, and Mo contents. The models were
152 trained using a suite of environmental predictors, including topographic features (DEM, slope, aspect), climate variables
153 (MAT, MAP, AI), vegetation indices (NDVI, NPP), soil properties (texture, SOC, pH, CIA), and ~~anthropogenic disturbance~~
154 ~~(grazing intensity)~~. Random forest was selected for its ability to model complex, nonlinear relationships and interactions
155 among diverse types of predictors. Model hyperparameters were optimized using grid search combined with tenfold

156 cross-validation. To assess model generalizability, we examined the extent to which the predictor parameter space in the
 157 validation set overlapped with that of the original training data. Model performance was evaluated by comparing predicted
 158 versus observed values using scatterplots (predicted on the x-axis, observed on the y-axis) following the method of Piñeiro et
 159 al. (2008), with models achieving strong predictive performance ($R^2 = 0.6-0.7$). The uncertainty layer is calculated as the
 160 inter-pixel variance among tree predictions. All statistical analyses were conducted using R version 3.4.4.

161 3 Results

162 3.1 Soil micronutrients contents ~~elements~~ ranking

163 Across all sites, soil micronutrient contents varied widely, with mean value of $22,864.30 \pm 7,589.01$ for Fe (mean \pm SD,
 164 $\text{mg}\cdot\text{kg}^{-1}$), 576.74 ± 206.44 for Mn, 25.32 ± 9.28 for Cu, 27.24 ± 8.55 for Zn, 49.35 ± 10.98 for Ni, 56.99 ± 19.33 for V, and
 165 4.63 ± 1.14 for Mo. Coefficients of variation ($\text{CV} = \text{SD}/\text{mean}$) were 33% for Fe, 36% for Mn, 37% for Cu, 31% for Zn, 22%
 166 for Ni, 34% for V and 25% for Mo. Collectively, Fe and Mn dominate in absolute abundance, whereas Cu-Zn-Ni-V occur at
 167 tens of $\text{mg}\cdot\text{kg}^{-1}$ and Mo remains low ($\sim 5 \text{ mg}\cdot\text{kg}^{-1}$), indicating heterogeneous but orderly micronutrient levels across the
 168 Plateau (Figs. 2 and S5).



169 **Figure 2.** Frequency distributions of soil micronutrients (Fe, Mn, Cu, Zn, Ni, V) across the Tibetan Plateau. ~~Content hierarchy and~~
 170 frequency distributions of soil microelements (Fe, Mn, Cu, Zn, Ni, Mo) across the Tibetan Plateau. (a) Elemental ranking by mean content,
 171 (b-g) Frequency distribution histograms for each microelement showing spatial heterogeneity patterns.

173 3.2 Soil micronutrients ~~microelements~~ across ~~vegetation~~ Vegetation types

174 Soil micronutrients ~~microelements~~ contents (Fe, Mn, Cu, Zn, Ni, V, and Mo) varied significantly among different vegetation
 175 types (Figs. 3 and S6). Fe contents were highest in shrub and forest ecosystems, with mean values of $26,264.11 \text{ mg}\cdot\text{kg}^{-1}$ and

176 26,090.66 mg·kg⁻¹, respectively, significantly exceeding values observed in desert (19,762.66 mg·kg⁻¹) and steppe
177 ecosystems (19,852.37 mg·kg⁻¹) by 31-33%. Similarly, Mn contents were greatest in forest (703.22 mg·kg⁻¹) and cropland
178 (608.29 mg·kg⁻¹), followed by shrub (606.33 mg·kg⁻¹) and meadow (591.59 mg·kg⁻¹), while the lowest Mn levels were
179 recorded in desert and steppe ecosystems (both below 510 mg·kg⁻¹).

180 Soil Cu showed minimal variation across vegetation types, with mean values ranging narrowly between 25.23 and
181 31.1425.91 mg·kg⁻¹. CroplandForest soils had slightly higher Cu levels, but the differences were not statistically significant,
182 suggesting a relatively uniform spatial distribution of Cu across ecosystems. Zn, however, demonstrated a strong
183 vegetation-dependent variability, with the highest mean contents found in forest (32.00 mg·kg⁻¹) and shrub (31.15 mg·kg⁻¹)
184 ecosystems. In contrast, Zn levels were markedly lower in steppe (22.94 mg·kg⁻¹) and desert (21.95 mg·kg⁻¹) soils, with
185 differences exceeding 10 mg·kg⁻¹, indicating pronounced biogeochemical variation.

186 In contrast to the previous elements, Ni and Mo exhibited distinct patterns across vegetation types, with notably lower
187 contents in forest and shrub ecosystems. Ni contents were highest in meadow soils (54.34 mg·kg⁻¹), followed by shrub
188 (52.66 mg·kg⁻¹), steppe (48.78 mg·kg⁻¹), cropland (48.22 mg·kg⁻¹), desert (43.87 mg·kg⁻¹), and forest ecosystems (41.73
189 mg·kg⁻¹). Soil Mo contents showed negligible differences among ecosystems, though steppe exhibited marginally higher
190 levels. No statistically significant differences were observed between vegetation types, indicating minimal vegetation control
191 over Mo distribution.

192 The highest soil V mean value occurred in forest soils (63.70 mg·kg⁻¹), followed by shrub (61.94 mg·kg⁻¹) and cropland
193 ecosystems (60.02 mg·kg⁻¹). These values were markedly greater than those observed in steppe (50.22 mg·kg⁻¹) and desert
194 (52.80 mg·kg⁻¹) soils, with differences reaching up to 25%. Meadow soils showed intermediate V levels (56.07 mg·kg⁻¹).
195 Statistical comparisons revealed that V contents in forest and shrub ecosystems were significantly higher than those in steppe
196 and meadow ecosystems (p < 0.05).

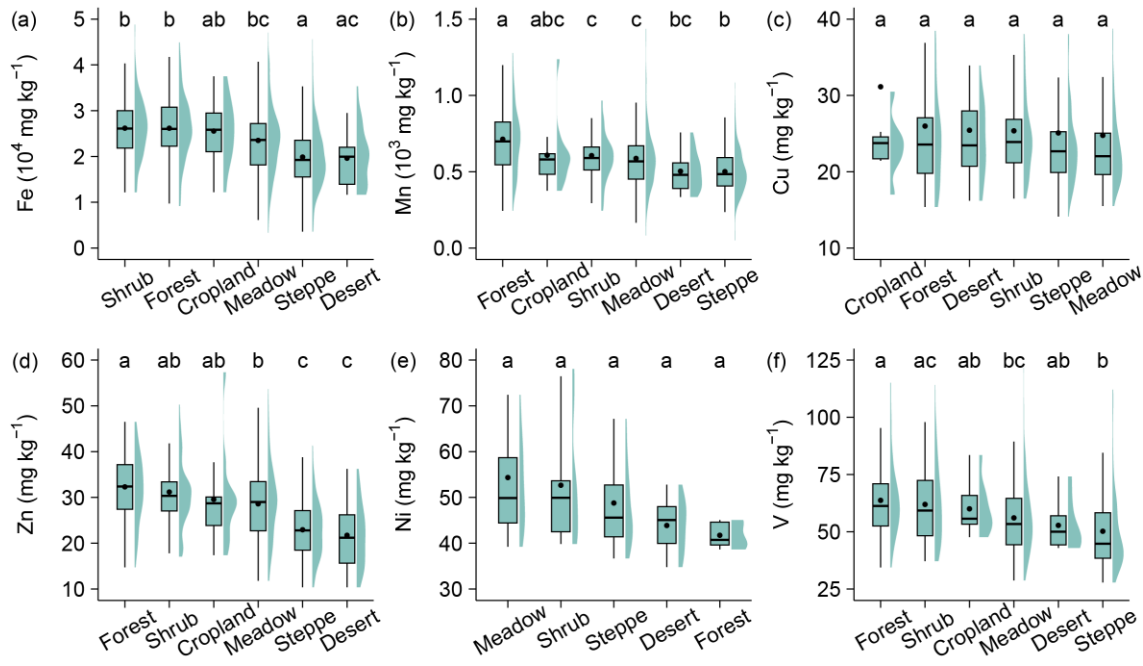
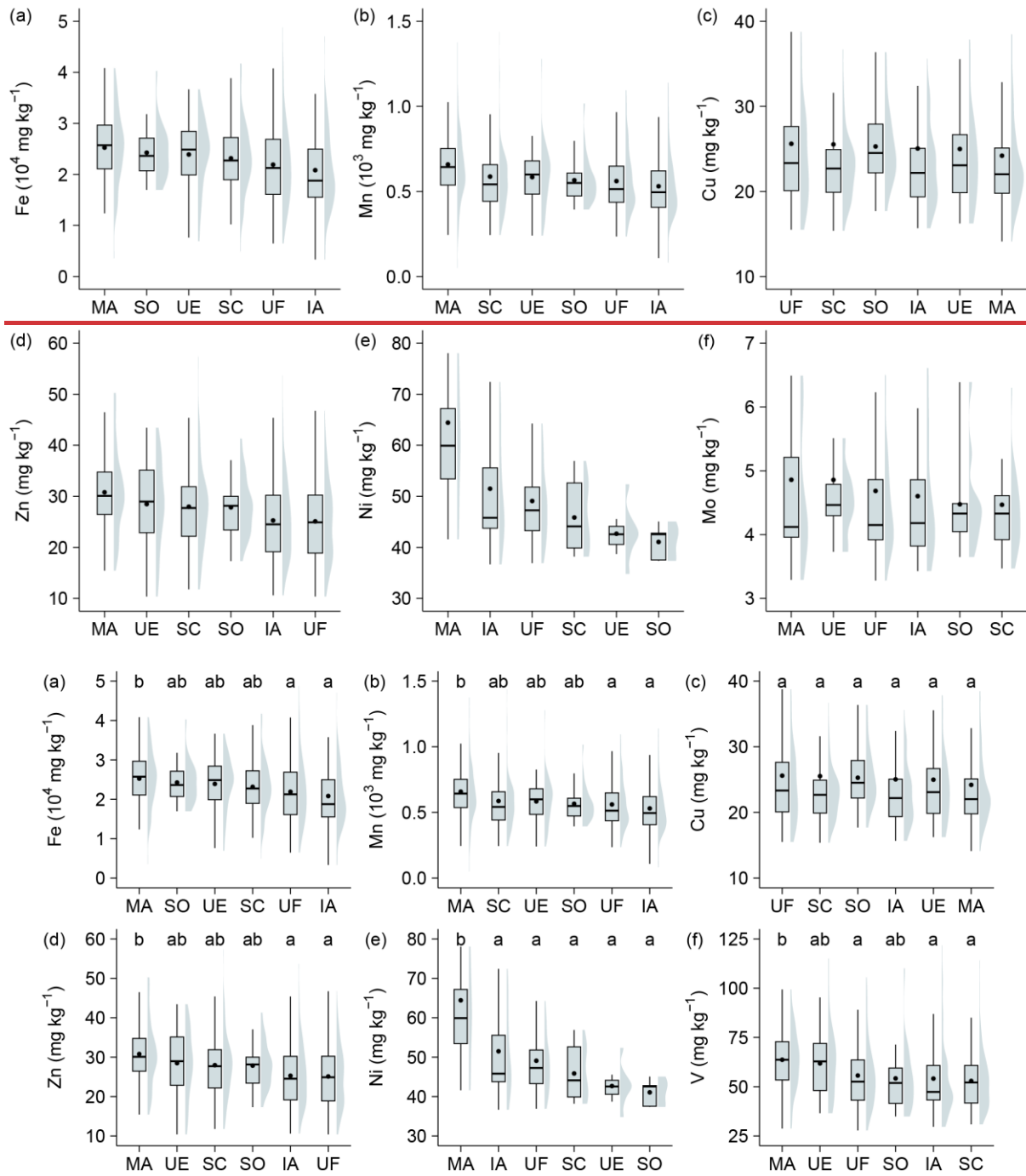


Figure 3. Variability in soil micronutrient/microelement contents (Fe, Mn, Cu, Zn, Ni, V, Mo) across Tibetan vegetation types. Boxplots show the data distributions for each vegetation type. Within each plot, the boxes represent the interquartile range (IQR), the horizontal lines within boxes indicate the median values, and black dots denote the mean values. The whiskers extend to 1.5 times the IQR. The surrounding shaded violin shapes indicate the kernel density distribution of the data. Lowercase letters denote significance groups from Tukey's HSD multiple comparisons ($\alpha = 0.05$): groups sharing at least one letter do not differ significantly, whereas groups with no letters in common differ significantly (e.g., "ab" is not different from "a" or "b").

3.3 Soil micronutrients/microelements across lithological classes

Lithological class exerted a significant influence on the spatial distribution of certain soil micronutrients/microelements (Figs. 4 and S7). Fe contents differed notably across lithological classes, with the highest values observed in soils derived from acidic metamorphic rocks (mean value: $25,252.72 \text{ mg}\cdot\text{kg}^{-1}$), followed by those from carbonate rocks ($24,260.96 \text{ mg}\cdot\text{kg}^{-1}$) and eolian facies rocks ($23,902.77 \text{ mg}\cdot\text{kg}^{-1}$). The lowest Fe contents were recorded in soils developed from acidic igneous rocks ($20,830.15 \text{ mg}\cdot\text{kg}^{-1}$). A similar geochemical pattern was observed for Mn, with the maximum contents in acidic-metamorphic-driven soils ($658.37 \text{ mg}\cdot\text{kg}^{-1}$), and the lowest in acidic-igneous-driven soils ($530.45 \text{ mg}\cdot\text{kg}^{-1}$).

Zn contents in soils also varied across lithologies, with the highest values associated with acidic metamorphic rocks (mean value of $30.79 \text{ mg}\cdot\text{kg}^{-1}$), followed by eolian facies rocks and clastic sedimentary rocks, while relatively lower levels were found under acidic igneous rocks ($25.27 \text{ mg}\cdot\text{kg}^{-1}$) and fluvial facies rocks ($25.10 \text{ mg}\cdot\text{kg}^{-1}$). In contrast, Cu and Mo showed no significant differences among lithological classes. Cu contents were slightly higher under fluvial facies rocks ($25.60 \text{ mg}\cdot\text{kg}^{-1}$), but overall differences were minimal. Similarly, Mo contents were relatively uniform, with slightly elevated levels under acidic metamorphic rocks and eolian facies rocks (both $\sim 4.86 \text{ mg}\cdot\text{kg}^{-1}$), and lower values under clastic sedimentary rocks and carbonate rocks (both $< 4.48 \text{ mg}\cdot\text{kg}^{-1}$), though differences were not statistically significant.



218

219

220 **Figure 4.** Variability in soil ~~micronutrient/micrelement~~ contents (Fe, Mn, Cu, Zn, Ni, ~~V,Mo~~) across Tibetan lithological classes. Boxplots
 221 show the data distributions for each lithological classes. Within each plot, the boxes represent the interquartile range (IQR), the horizontal
 222 lines within boxes indicate the median values, and black dots denote the mean values. The whiskers extend to 1.5 times the IQR. The
 223 surrounding shaded violin shapes indicate the kernel density distribution of the data. Lowercase letters denote significance groups from
 224 Tukey's HSD multiple comparisons ($\alpha = 0.05$): groups sharing at least one letter do not differ significantly, whereas groups with no letters
 225 in common differ significantly (e.g., "ab" is not different from "a" or "b"). Abbreviations of lithological classes: IA = acidic igneous rock,
 226 MA = acidic metamorphic rock, SC = clastic sedimentary rock, SO = carbonate rock, UE = eolian facies rock, UF = fluvial facies rock.

227 Soil Ni contents showed the most pronounced variation among lithologies, with the highest level recorded under acidic
 228 metamorphic rocks ($64.43 \text{ mg}\cdot\text{kg}^{-1}$), followed by acidic igneous rocks ($51.49 \text{ mg}\cdot\text{kg}^{-1}$). Soils developed from clastic

229 sedimentary rocks and carbonate rocks had significantly lower Ni contents (45.85 and 41.06 mg·kg⁻¹, respectively). The
230 highest V contents were found in soils derived from acidic metamorphic rocks (63.67 mg·kg⁻¹), followed by soils developed
231 from eolian facies rocks (61.81 mg·kg⁻¹) and fluvial facies rocks (55.67 mg·kg⁻¹). In contrast, soils originating from
232 carbonate (54.20 mg·kg⁻¹), acidic igneous (54.11 mg·kg⁻¹), and clastic sedimentary rocks (52.92 mg·kg⁻¹) exhibited
233 relatively lower V levels. In summary, Fe, Mn, Zn, and Zn-V were substantially enriched in soils derived from acidic
234 metamorphic rocks. Cu and Mo showed relatively uniform distributions across lithologies Ni was notably elevated under
235 acidic metamorphic rocks.

236 3.4 Drivers of soil micronutrient pattern

237 Relative importance analysis was conducted for five predictor groups, including climate, vegetation, soil properties,
238 topography, and grazing disturbances. The rankings show clear element-specific controls (Figs. 5a-f and S8). Soil properties
239 were the primary contributors to the spatial variation of micronutrient contents, followed by topographic and climatic factors,
240 whereas vegetation and anthropogenic disturbance had relatively minor effects. Among all predictors, the chemical index of
241 alteration, slope, and soil texture exhibited the highest importance, indicating that weathering intensity, terrain, and soil
242 physical structure are the dominant controls on the spatial distribution of soil micronutrients. Specifically, the chemical index
243 of alteration emerged as the dominant factor for Fe, Zn, and V. Topographic factors (slope) primarily influenced Mn, while
244 climatic variables (MAP, AI) and biological productivity (NPP) contributed more to Cu and Ni variations. Mo is mainly
245 influenced by the soil texture.

246 ~~Relative importance analysis considered five variable groups, including climate, vegetation, soil properties, topography, and~~
247 ~~human disturbances. Among all investigated variables, climatic factors dominantly control soil micronutrient (Fe, Mn, Cu,~~
248 ~~Zn, Ni) distribution across the Tibetan Plateau (Figs. 5a-f). Regional moisture conditions, characterized by mean annual~~
249 ~~precipitation (MAP) and aridity index (AI), were the primary drivers. MAP consistently ranked as the top predictor for Fe,~~
250 ~~Mn, Zn, and Ni. Vegetation indicators (e.g., NDVI, NPP) also showed high importance for Mo and Zn. Soil properties (pH,~~
251 ~~SOC, texture) and topography (slope, aspect, elevation) contributed to distribution patterns but exhibited lower relative~~
252 ~~importance.~~

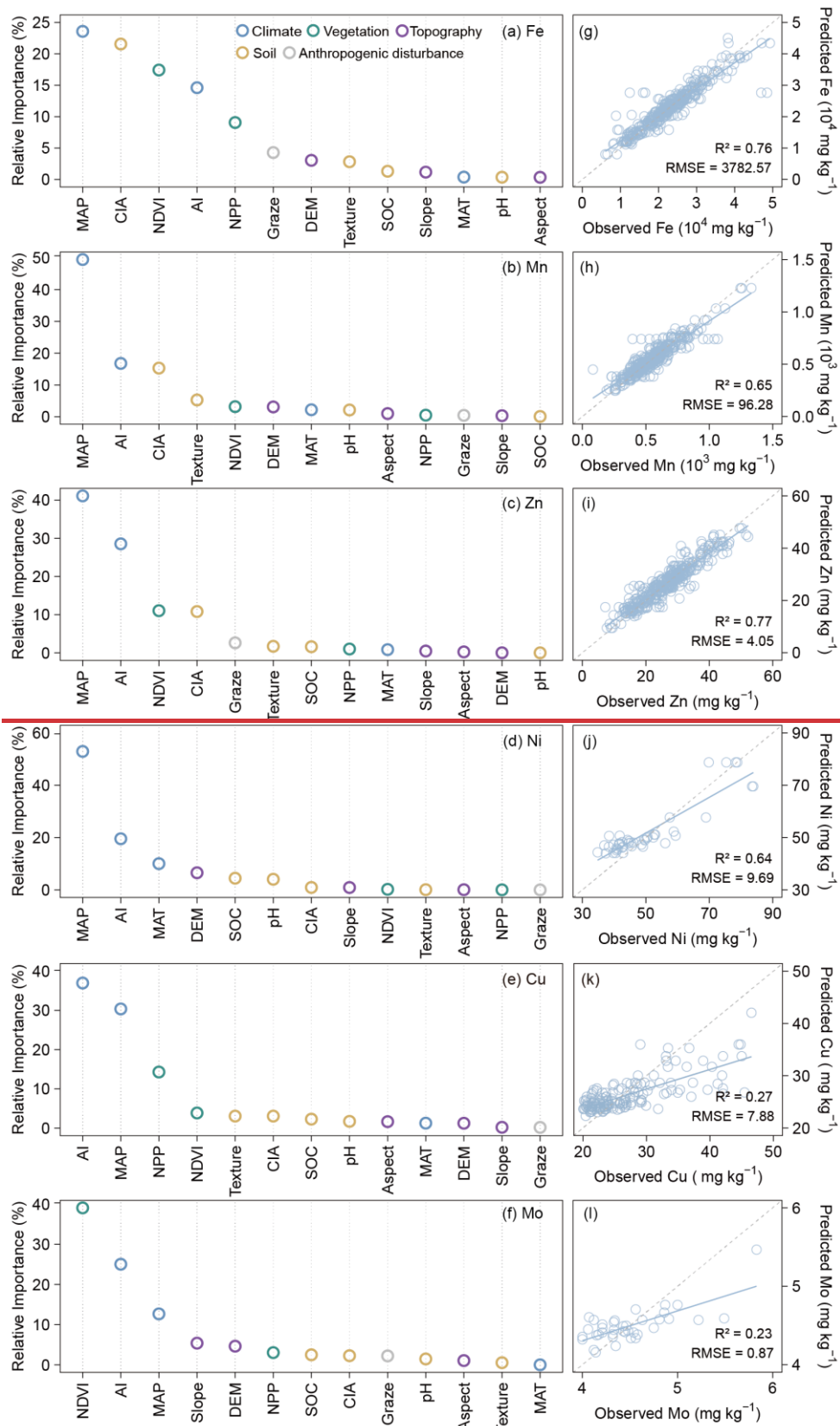
253 The partial dependence plots illustrated the nonlinear responses of seven soil micronutrients (Fe, Mn, Cu, Zn, Ni, V, and Mo)
254 to five key environmental variables (Figs. 6 and S9). Overall, the effects of the chemical index of alteration, soil texture,
255 slope, and aridity index varied substantially among elements. The chemical index of alteration showed a generally positive
256 relationship with most micronutrients, particularly Fe, Mn, Zn, V, and Mo, which increased markedly when chemical index
257 of alteration exceeded approximately 0.5. Soil texture exerted a moderate positive influence on micronutrients. In contrast,

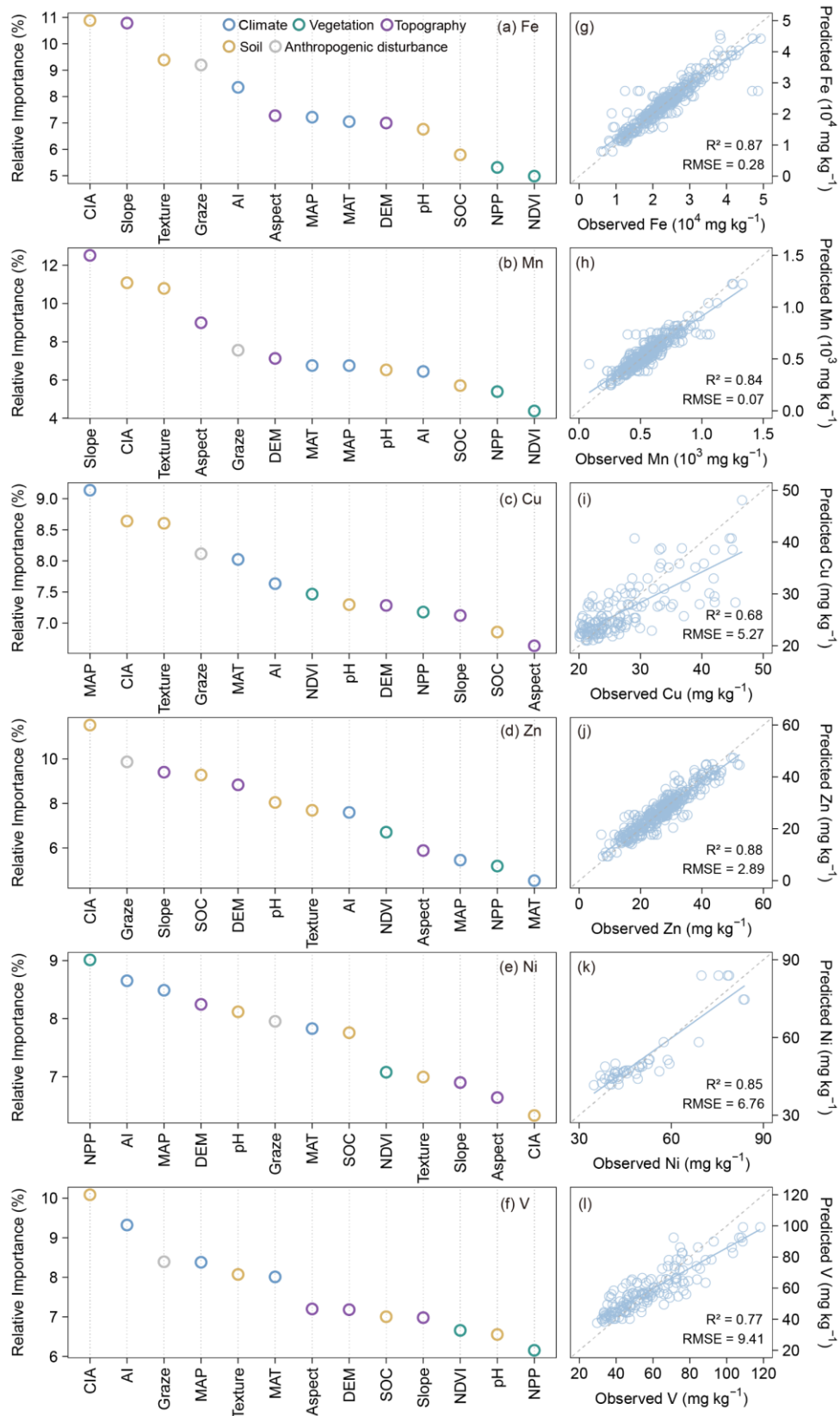
258 slope exhibited a saturating effect—nutrient concentrations rose sharply at low slope angles (<10°) and plateaued
259 thereafter—highlighting the limited accumulation potential on steeper terrains. The aridity index demonstrated a clear
260 U-shaped pattern for most micronutrients (Fe, Mn, Cu, Zn, Ni, V, and Mo), with relatively low concentrations under
261 intermediate aridity. Seven micronutrients (Fe, Mn, Cu, Zn, Ni, V, and Mo)The distribution of Fe was primarily regulated by
262 climatic conditions (especially precipitation) and parent material weathering intensity (represented by the chemical index of
263 alteration, CIA), with secondary contributions from normalized difference vegetation index (NDVI), aridity index (AI), net
264 primary productivity (NPP). For Mn distribution, Climate (MAP, AI) and soil properties (CIA, soil texture) were dominant.
265 Soil Zn also show highly sensitive to climate (MAP, AI), weathering intensity (CIA), and vegetation cover (NDVI). Ni
266 distribution was predominantly controlled by natural environmental conditions including MAP, AI, MAT and topography.
267 For both Cu and Mo, climate variables (AI, MAP) and vegetation indicators (NPP or NDVI) consistently ranked among the
268 top three factors governing their spatial distribution.

269 The partial dependence plots revealed distinct responses of soil microelement to key environmental drivers (Fig. 6). Five
270 elements (Fe, Mn, Cu, Zn, Ni) exhibited a typical U-shaped relationship with mean annual precipitation, showing higher
271 contents in both low and high precipitation zones, and a clear trough in the intermediate range (approximately 300–500
272 millimeters). This pattern aligned closely with responses to drought indices, confirming shared moisture sensitivity.

273 Collectively, these patterns emphasize that soil micronutrient distributions across the Tibetan Plateau are strongly shaped by
274 interactions among chemical weathering intensity, soil physical properties, and climatic aridity.

275 Increases in the chemical index of alteration were generally associated with elevated levels of Mn, Ni, and Cu, particularly
276 when the chemical index of alteration exceeded 0.5. In summary, the spatially heterogeneous distribution of Tibetan soil
277 microelements is co-regulated by precipitation, vegetation, and chemical weathering intensity.





279

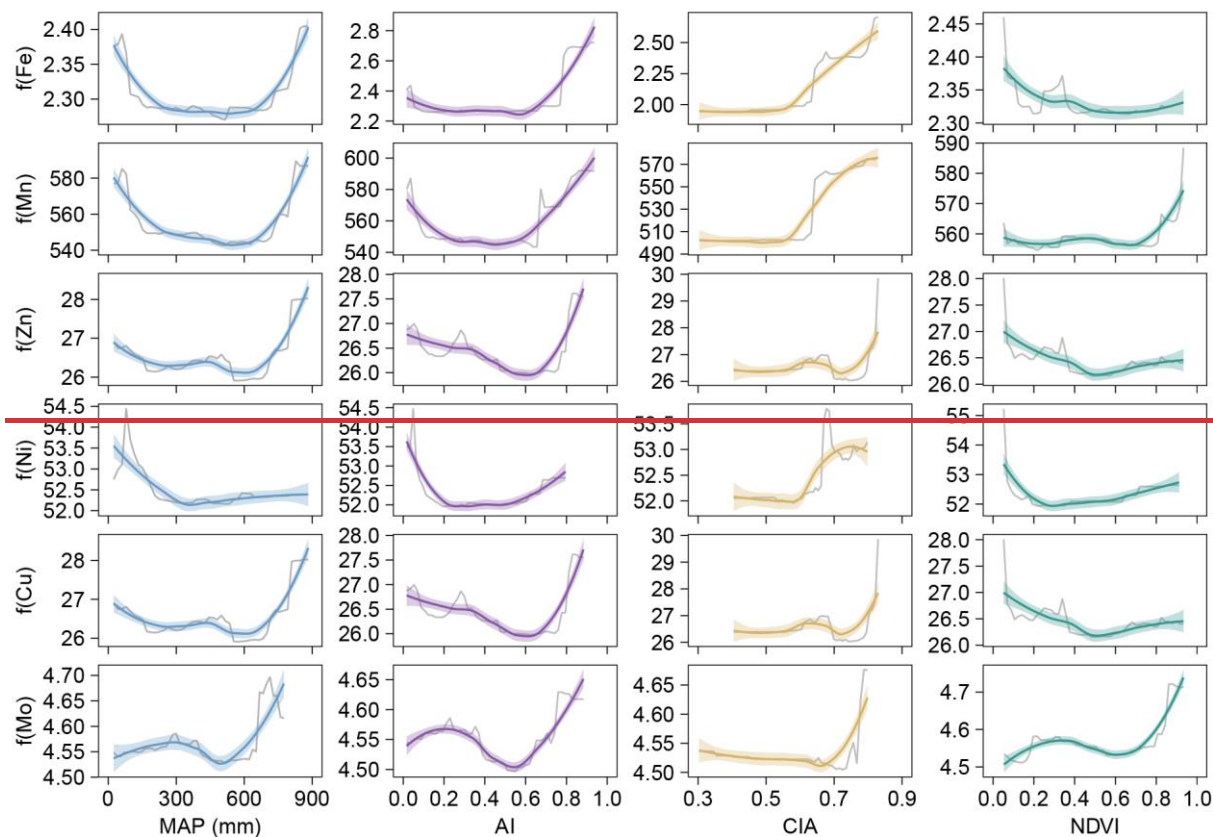
280

281

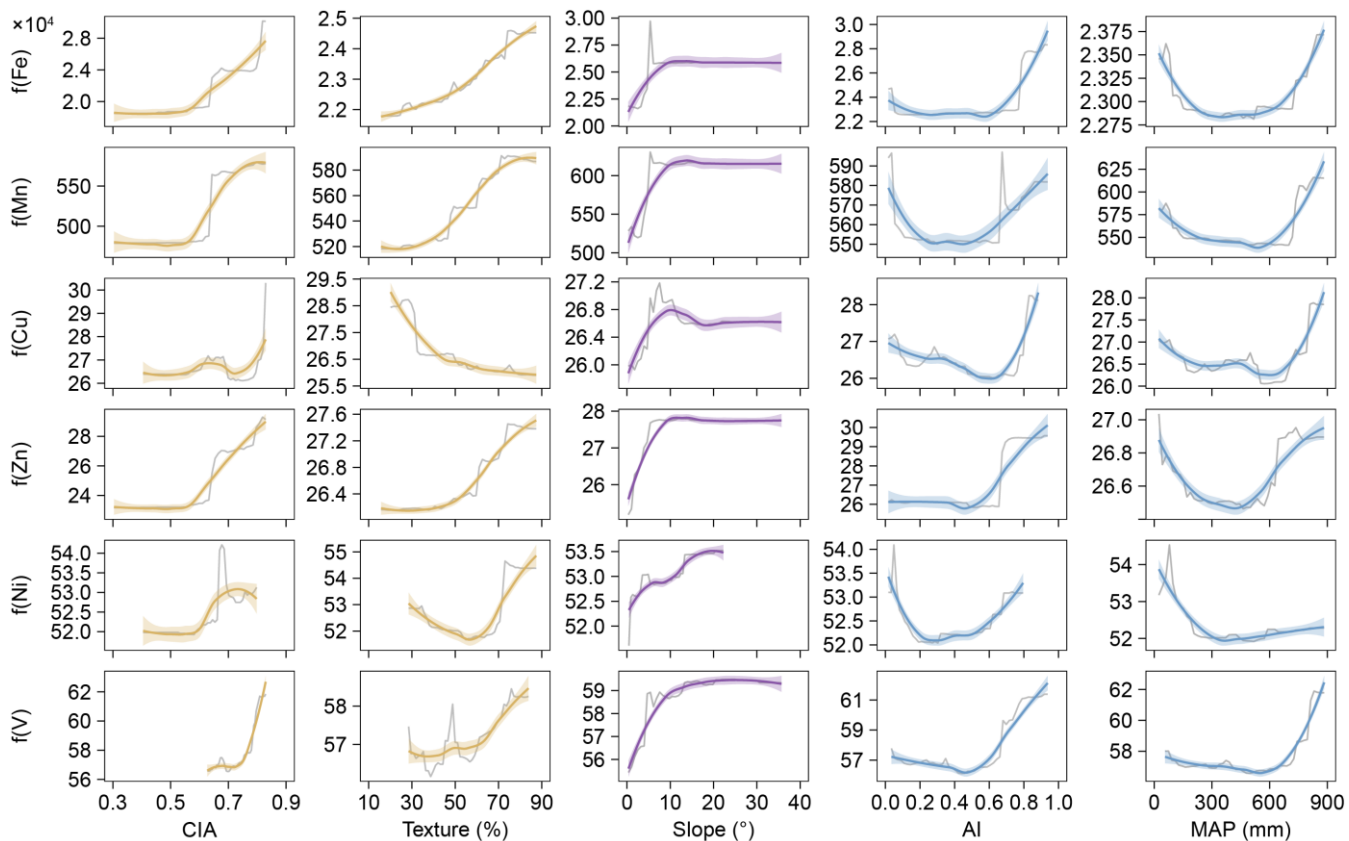
282

Figure 5. Relative importance of biotic and abiotic factors for soil micronutrients (Fe, Mn, Cu, Zn, Ni, V) microelements (Fe, Mn, Zn, Ni, Cu, Mo) on the Tibetan Plateau (a-f). Relationship between observed and predicted values of soil micronutrients (Fe, Mn, Cu, Zn, Ni, V) (Fe, Mn, Zn, Ni, Cu, Mo) on the Tibetan Plateau based on the Random Forest model (g-l). The blue solid line represents the fitted

283 relationship using ordinary least squares regression, while the gray dashed line indicates the 1:1 line between observed and predicted
 284 values.



285



286

287 **Figure 6.** Partial dependence of six soil micronutrients (Fe, Mn, Cu, Zn, Ni, V)~~microelements (Fe, Mn, Zn, Ni, Cu, Mo)~~ on four predictive
288 variables: chemical index of alteration (CIA), Texture, Slope, aridity index (AI) and mean annual precipitation (MAP)~~mean annual~~
289 precipitation (MAP), aridity index (AI), chemical index of alteration (CIA), and normalized difference vegetation index (NDVI). Gray
290 lines represent the original partial dependence, while smoothed fits for each micronutrient~~element~~ are shown as colored lines. Shaded areas
291 represent the 95% confidence intervals.

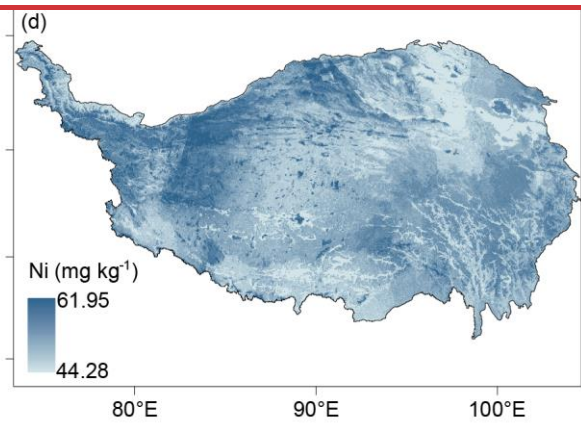
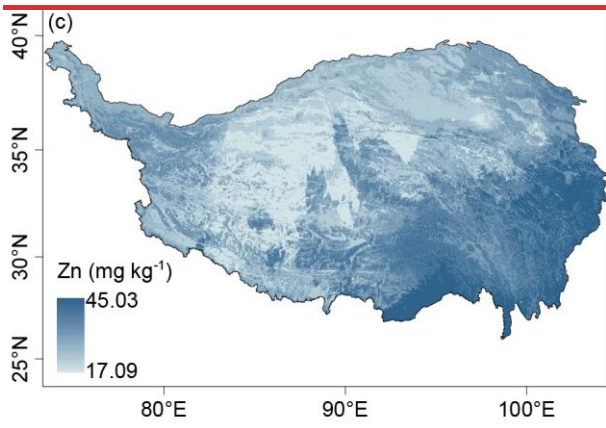
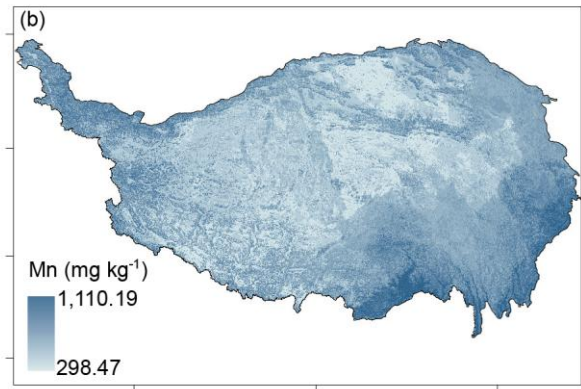
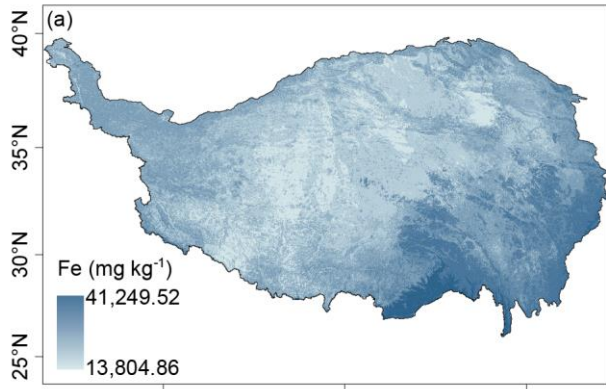
292 3.5 Soil micronutrients maps

293 The random forest (RF) models exhibited strong overall predictive performance for soil micronutrient concentrations across
294 the Tibetan Plateau, with varying accuracies among elements (Figs. 5g-l and S8). The models for Fe, Mn, Zn, Ni, and Mo
295 performed best, with R² values ranging from 0.83 to 0.88 and relatively low RMSE, indicating high consistency between
296 observed and predicted values. In particular, Zn (R² = 0.88) and Fe (R² = 0.87) achieved the highest predictive accuracy,
297 suggesting that their spatial variability is well captured by the selected environmental predictors. Mo (R² = 0.83), Mn (R² =
298 0.84) and Ni (R² = 0.85) also showed strong model fits, reflecting robust representation of their spatial patterns. The Cu and
299 V models displayed slightly lower but still acceptable performance (R² = 0.68 and 0.77, respectively), implying that
300 additional predictors may be required to fully capture their local variability. Overall, these results demonstrate that the
301 random forest models effectively predict the spatial distributions of major soil micronutrients, with particularly high
302 reliability for Fe, Mn, Zn, and Ni.

303 ~~We employed random forest modeling to predict the spatial distribution of six soil micronutrients across the Tibetan Plateau.~~
304 ~~Model performance varied among elements (Figs. 5g-l). The model achieved the highest predictive accuracy for Zn and Fe,~~
305 ~~with R² values of 0.77 and 0.76, respectively (Figs. 5g and 5i), indicating that the spatial variability of Zn and Fe is well~~
306 ~~captured by the selected environmental predictors. Mn and Ni models also showed moderate performance, with R² values of~~
307 ~~0.65 and 0.64 and corresponding RMSEs of 96.28 and 9.69 (Figs. 5h and 5j). In contrast, the models for Cu and Mo~~
308 ~~displayed poor predictability, with R² values of only 0.27 and 0.23 (Figs. 5k and 5l). Overall, the model evaluation results~~
309 ~~suggest that the random forest approach is effective in predicting the distributions of Fe and Zn, moderately reliable for Mn~~
310 ~~and Ni, and limited utility for Cu and Mo.~~

311 **Figure 7 and Figure S10** illustrates the spatial patterns of soil micronutrients (Fe, Mn, Cu, Zn, Ni, V, and Mo)~~microelements~~
312 (Fe, Mn, Zn, Ni) across the Tibetan Plateau, as predicted by random forest models. The resulting maps reveal significant
313 spatial heterogeneity of these elements. The highest contents of Fe are primarily located in the southeastern region, the
314 southern margins, and parts of the western plateau. Mn shows a distinct gradient, with contents increasing from northeast to
315 southwest. Predicted Mn values range from 298.47 to 1,110.19 mg·kg⁻¹, and the areas with the highest Mn contents are
316 mainly distributed in the humid southeastern and southern parts of the plateau. Cu ranges from 21.42 to 35.78 mg·kg⁻¹, with
317 relatively higher contents over the western-northern interior and highlands and lower values in the humid southeastern

318 valleys and along the southern margin. Zn displays relatively high contents in the central-eastern region and along certain
319 western edges of the plateau, with predicted values ranging from 17.09 to 45.03 mg·kg⁻¹. Ni has a narrower predicted
320 content range (44.28–61.95 mg·kg⁻¹) and shows a more spatially homogeneous distribution. However, localized hotspots of
321 elevated Ni contents are observed in parts of the northeastern and southern plateau. Predicted V contents ranged from 40.79
322 to 82.00 mg·kg⁻¹, displaying a clear spatial gradient. Higher contents were predominantly found in the southeastern and
323 southern regions of the plateau, where humid climatic conditions and intense chemical weathering promote V enrichment.
324 Moderate levels occurred across the central and eastern plateau, while the lowest concentrations were observed in the arid
325 western and northern areas. In contrast, Mo varies within a narrower interval (3.88-5.87 mg·kg⁻¹) and exhibits a weak
326 plateau-wide gradient, with slight enrichment on the northern plateau/basin areas and comparatively lower levels toward the
327 southeast.



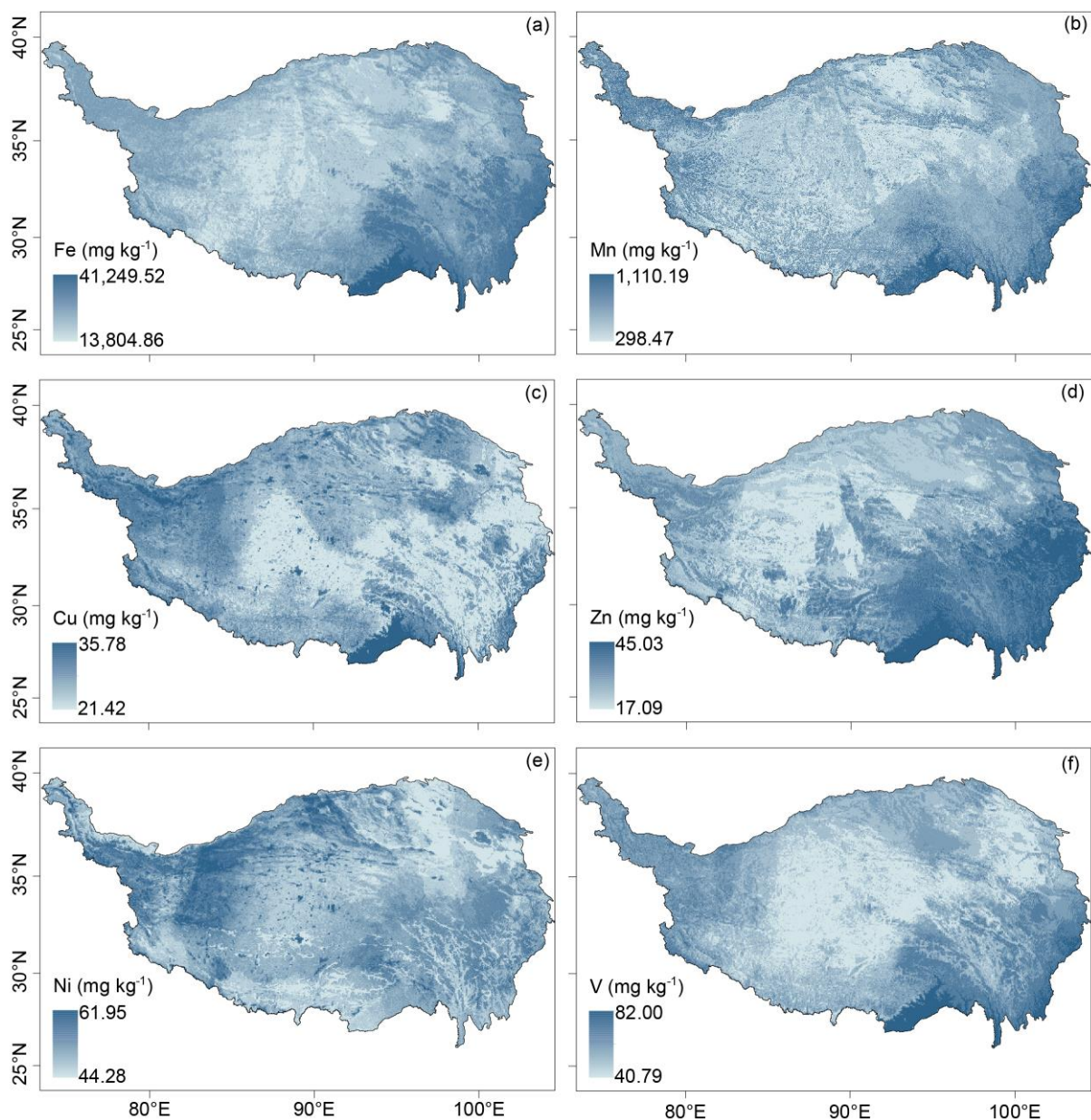


Figure 7. Spatial distribution of soil micronutrients (Fe, Mn, Cu, Zn, Ni, V) microelements (Fe, Mn, Zn, Ni) on the Tibetan Plateau.

4 Discussion

We added comparisons of our results with the few available observations on the Tibetan Plateau, as well as broader datasets from other regions, to better place our findings in a wider context (Table S1). In terms of data range and mean values, the contents and magnitudes of the soil micronutrients we observed are generally consistent with previous reports from the Plateau and global grassland soils, indicating the reliability of our datasets. For the Plateau, the mean Zn, and V contents in this study were slightly lower, while Ni were somewhat higher (Fig. S11). These discrepancies are more likely due to differences in study regions. Our sampling covered a much broader area, whereas previous studies focused mainly on local regions such as the Heihe Basin (Bu et al., 2016). Given the substantial spatial heterogeneity of soil micronutrients across the

340 Tibetan Plateau, such differences are expected and further highlight the necessity of exploring soil micronutrient patterns at
341 the plateau scale. Our results indicate generally low contents of soil micronutrients (Fe, Mn, Cu, Zn, Ni, Mo) across Tibetan
342 Plateau ecosystems (Fig. 2), consistently falling below well-established global averages for reference soils (Lindsay 1979).
343 These deficient levels carry profound long-term ecological implications, including the risk of irreversible depletion of
344 lithogenic microelement pools (Jones et al. 2013), given their replenishment cycles operate on geological timescales (million
345 years). Furthermore, accelerated warming may exacerbate microelement dilution effects, thereby increasing regional soil
346 degradation vulnerability (Clair & Lynch, 2010; Myers et al., 2014; Pachauri et al., 2014).

347 The distribution of soil micronutrients/microelements across the Tibetan Plateau demonstrates significant spatial
348 heterogeneity (Figs. 2, 7, S4, and S10-and-7), aligning with patterns observed in Europe for elements such as Zn (Van et al.,
349 2023). This variability is predominantly governed by the interactions among soil, topography, and climate (Figs. 5a-f, 6 S8
350 and S9). Soils act as the principal sink for micronutrients entering the terrestrial environment through both natural processes
351 and anthropogenic inputs. Consistent with continental-scale assessments, clay content emerged as the dominant control on
352 the spatial distribution of soil Zn in Europe, with coarse-textured soils showing markedly lower Zn concentrations (Van et al.,
353 2023). Similar texture effects have been reported for other elements: soil Cu is positively related to clay and negatively
354 related to sand (Ballabio et al., 2018), sensitivity analyses show that soil Se increases with increasing clay (Jones et al.,
355 2017), whereas surface-soil Hg decreases once sand exceeds ~30 % (Ballabio et al., 2021). These patterns agree with our
356 observation that ecosystems developed on coarse substrates contain the lowest levels of micronutrients. This is because clay
357 serves as an adsorption site for metal elements, whereas sandy soils are relatively weak adsorbents for micronutrients
358 (Mesquita, 1998). In poorly developed soils with low clay content, such as those in arid climates, the lack of capacity to
359 retain soil organic matter leads to a significant reduction in the amount of micronutrients, making them less likely to
360 accumulate (Moreno-Jimenez et al., 2019). In addition to soil properties, factors such as topography also play a significant
361 role in the micronutrient content of surface soils on the Tibetan Plateau. Elevation-related variations in soil micronutrient are
362 limited, and some elements (e.g., Cu, Mo) remain relatively stable; Fe, Mn, Zn, and V show similar patterns, with higher
363 contents at lower elevations than at higher ones (Fig. S12 and S13). Contents of Fe, Mn, Zn, and V increased with slope
364 steepness, particularly below 10°, whereas Cu and Ni showed weaker or nonlinear trends. This pattern suggests that
365 topography governs both physical and chemical soil-forming processes by controlling erosion, leaching, and moisture
366 dynamics (Jenny, 1941; Montgomery, 2007). Steeper slopes enhance runoff and erosion, removing fine particles enriched in
367 Fe and Mn oxides and promoting elemental redistribution along hillslopes, while also accelerating bedrock weathering and
368 releasing lithogenic elements such as Fe and V (Yoo et al., 2006). In contrast, gentler slopes favor organic matter
369 accumulation and reducing conditions that can immobilize or leach redox-sensitive elements. Overall, slope-driven

370 variations in hydrology, weathering, and redox status collectively shape the spatial heterogeneity of soil micronutrients
371 across the Plateau (Quesada et al., 2010).
372 ~~climate, vegetation, and soil (Figs. 5a-f and 6).~~ Notably, precipitation emerges as the primary predictor for
373 ~~micronutrient~~elements such as Fe, Mn, Cu, Zn, V, and Mo~~Ni~~, with all ~~element~~except Mo exhibiting characteristic U-shaped
374 responses, with minima occurring at 300-500 mm. This pattern likely reflects distinct weathering regimes across
375 precipitation gradients. In arid regions (<300 mm), physical weathering processes, including freeze-thaw fracturing and
376 aeolian erosion, predominate, allowing ~~micronutrient~~trace elements (e.g., Ni, ~~Mo~~) to accumulate near the surface due to
377 evaporation effects (Pachauri et al., 2014; Moreno-Jimenez et al., 2023). In transitional precipitation regimes (300-500 mm),
378 intensified chemical weathering occurs; however, leaching fluxes surpass the rates of parent material weathering, leading to
379 soil elemental depletion (Anderson, 2019; Bluth et al., 1994; Hartmann et al., 2014). In humid regions (>500 mm), enhanced
380 chemical weathering results in the formation of secondary clay minerals (e.g., montmorillonite, illite), whose negatively
381 charged surfaces facilitate elemental retention through ionic adsorption and co-precipitation mechanisms (Alloway, 2009).
382 To further verify these nonlinear effects, accumulated local effects (ALE) analyses were performed and revealed consistent
383 U-shaped responses for Fe, Mn, Cu, Zn, V, and Mo, confirming the robustness of the partial dependence results (Figs. S14
384 and S15). This pattern likely reflects a trade-off between weathering intensity, leaching losses, and elemental retention under
385 contrasting hydrological conditions. Additionally, MAP showed a significant positive correlation with the chemical index of
386 alteration (Fig. S16), indicating that higher precipitation enhances chemical weathering. However, this relationship alone
387 does not fully explain the observed U-shaped nutrient responses, as direct indicators of leaching fluxes and mineral retention
388 are lacking. We therefore consider this U-shaped pattern, supported by multiple lines of evidence, as an open question for
389 future investigation, emphasizing the need for complementary datasets (e.g., redox status, mineral composition) to refine its
390 mechanistic interpretation. Although lithological differences are detectable for some elements, they do not alter the overall
391 spatial patterns (Figs. 4 and S7). In summary, lithology modulates the baseline levels of certain micronutrients but is not the
392 dominant factor shaping their regional distributions, which are more strongly governed by external environmental drivers
393 such as climate, weathering intensity, sediment transport, and biotic cycling.
394 Our findings suggest that the aridity index is a significant determinant of soil ~~micronutrient~~microelement distribution.
395 Specifically, elemental contents tend to decrease when the aridity index falls below a certain threshold (Figs. 6 and S9). This
396 trend likely reflects reduced input or retention of elements under arid conditions. Grouped comparisons across aridity classes
397 (humid, dry sub-humid, semi-arid, arid, and hyper-arid) were performed. The results show that the medians and means of Fe,
398 Mn, Cu, Zn, Ni, V, and Mo decrease with increasing aridity, with the largest declines observed for Fe, Mn, Zn, and V (Fig.
399 S17 and S18). Drought conditions may modify soil redox states, thereby influencing element speciation, adsorption capacity,

400 mobility, and ultimately, leaching behavior (Brady et al., 2016; Loveland et al., 2003; Carter et al., 1995). Also, arid
401 environments may indirectly impact micronutrients trace elements through alterations in soil pH and soil organic matter
402 content (Moreno-Jimenez et al., 2019). Previous research has shown that droughts induced by climate change can restrict the
403 availability of essential micronutrients microelements, such as iron and zinc. This limitation, along with other adverse effects
404 like diminished water availability, poses substantial threats to vital ecological processes and services in drylands, including
405 food production (Gupta et al., 2008; Graham, 1991). Furthermore, ongoing regional warming and associated hydroclimatic
406 shifts may interact with hydrology and redox processes, organic-matter cycling, and vegetation patterns, thereby altering the
407 availability and spatial variability of certain micronutrients (Myers et al., 2014; Pachauri et al., 2014).
408 Multiple biogeochemical processes are sensitive to micronutrient availability. Biological nitrogen fixation relies on Mo and
409 Fe as essential cofactors of nitrogenase, while the methane cycle depends on Ni and Cu through their roles in
410 methanogenesis and methane oxidation, respectively (Thauer et al., 2019; Stefan et al., 2020). Permafrost thaw and
411 thermokarst development can further activate Fe-Mn redox cycling, altering metal mobility (Chauhan et al., 2024).
412 Collectively, soil micronutrients depletion may cascade through nutrient cycling and ecosystem feedbacks, amplifying the
413 impacts of ongoing environmental change across the Plateau.

414 **5 Uncertainty**

415 Although the laboratory XRF measurements used in this study were validated against ICP-MS and generally showed strong
416 correlations, several limitations should be noted. For Fe, Mn, V and Cu, the two methods produced highly consistent results,
417 supporting the robustness of the dataset. In contrast, Zn and Ni, exhibited systematic deviations from the 1:1 line, with XRF
418 tending to slightly over- or underestimate contents relative to ICP-MS (Fig. S1). These deviations likely arise from
419 element-specific detection sensitivities of XRF. To address this, we calibrated Zn and Ni, using the regression relationships
420 between the two methods and then repeated spatial mapping. The results before and after calibration were not significantly
421 different, confirming that these deviations do not affect our main findings (Figs. S2 and S3). For Mo, the results obtained
422 from the two methods were not fully consistent, likely due to its low content (Fig. S4). The XRF-based measurements may
423 involve considerable uncertainties. Nonetheless, we acknowledge that incorporating ICP-based measurements on a larger
424 sample set would further strengthen the accuracy of the dataset, and future efforts should consider combining multiple
425 analytical approaches to minimize methodological uncertainties.

426 Our random forest regression models demonstrated robust predictive capability (e.g. cross-validated R^2 range from 0.64 to
427 0.77 for Fe Mn Zn Ni; Table S2). Cu and Mo exhibit weaker predictive performance, which may be attributed to the

428 following reasons: First, analytical limitations may introduce measurement error, as both elements occur at very low contents,
429 especially Mo. Second, key process controls are not fully captured by the current predictors. E.g. Cu is strongly influenced
430 by nonlinear interactions with Fe/Al oxides, whereas Mo is affected by carbonate content, redox conditions (Tack et al.,
431 1995). These mineralogical and redox variables are underrepresented, leading to potential bias. In addition, both elements
432 show hotspot-prone, right-skewed distributions (Figs. 2 and S5), likely due to localized anthropogenic sources. The spatial
433 predictions inevitably contain uncertainties arising from both the Random Forest model and the input datasets. Model-based
434 uncertainty was quantified as the inter-tree variance among predictions (RF-SD; Figs. S11 and S12), while additional
435 uncertainty may stem from sparse meteorological observations and limited soil sampling across the Tibetan Plateau.
436 Nevertheless, model accuracy could be further improved to more extensive field sampling and refinement of input data.
437 Specifically, targeted collection of soil microelement data and associated covariates in underrepresented high-altitude regions
438 of the Tibetan Plateau is necessary to address existing spatial gaps. Additionally, systematic reduction of uncertainties
439 inherent in gridded environmental datasets is essential, as these uncertainties propagate errors into microelement predictions.
440 Continued advancement in both field observations and foundational geospatial dataset is crucial for improving the reliability
441 of regional-scale element mapping.

442 We note that ecosystem-specific pedogenesis (e.g., organic-rich surface layers in some forests vs. thin mineral A horizons in
443 grasslands) can contribute to differences in surface micronutrient contents. Consequently, part of the spatial variation we
444 report likely reflects vertical horizon contrasts sampled at a uniform 0-10 cm depth. Users should consider this context when
445 applying the dataset, especially for process inference or when comparing across ecosystems with contrasting surface
446 horizons. Where applications require deeper profiles or horizon-specific interpretation, we recommend integrating our maps
447 with local profile data.

448 **6 Data availability**

449 The gridded soil micronutrient (Fe, Mn, Cu, Zn, Ni, V, and Mo)~~trace element (Fe Mn Zn Ni)~~ maps for Tibetan Plateau can be
450 downloaded from <https://doi.org/10.11888/Terre.tpcd.302870-303049> (Huo et al., 2025).

451 **6 Conclusions**

452 This study delivers a comprehensive assessment of spatial distribution patterns for seven~~six~~ soil micronutrients (Fe, Mn, Cu,
453 Zn, Ni, V, and Mo) across the Tibetan Plateau, revealing pronounced regional-scale heterogeneity. Soil properties were the
454 primary contributors to the spatial variation of micronutrient contents, followed by topographic and climatic factors, whereas

~~vegetation and grazing disturbance had relatively minor effects. Moisture-related variables (e.g., mean annual precipitation, aridity index) are the primary drivers of microelement distributions, with significant secondary modulation by weathering intensity and vegetation factors.~~ These findings highlight the coupled effects of climate, vegetation, and parent material on microelement biogeochemical cycling within the complex environmental context of the Tibetan Plateau. Using five predictor groups (climate, vegetation, soil properties, topography, and ~~grazing~~human disturbances), we generated high-resolution spatial maps for ~~key soil micronutrients (Fe, Mn, Cu, Zn, Ni, V, and Mo)~~four well-predicted elements (Fe, Mn, Zn, Ni) via machine learning. These maps provide validated initial conditions for process-based models simulating ~~micronutrient~~microelement cycling, advances understanding of elemental distribution in alpine ecosystems.

463 **Author contributions.**

464 JZ conceived the study. HY conducted the field survey and was responsible for data collection and processing. HY prepared
465 the manuscript with contributions from all co-authors.

466 **Competing interests.**

467 The contact author has declared that none of the authors has any competing interests.

468 **Acknowledgements.**

469 This study was supported by the Second Tibetan Plateau Scientific Expedition and Research Program (2022QZKK0101),
470 National Natural Science Foundation of China (42471159), and Chinese Academy of Sciences (CAS) Project for Young
471 Scientists in Basic Research (YSBR-037).

472 **Appendix A: Supplementary material**

473 **Appendix B: Metadata**

474 **References**

475 Alloway, B. J.: Soil factors associated with zinc deficiency in crops and humans, *Environmental Geochemistry and Health*,
476 31, 537-548, <https://doi.org/10.1007/s10653-009-9255-4>, 2009.

- 477 Anderson, S. P.: Breaking it down: Mechanical processes in the weathering engine, *Elements: An International Magazine of*
478 *Mineralogy, Geochemistry, and Petrology*, 15, 247-252, <https://doi.org/10.2138/gselements.15.4.247>, 2019.
- 479 Bluth, G. J., and Kump, L. R.: Lithologic and climatologic controls of river chemistry, *Geochimica et Cosmochimica Acta*,
480 58, 2341-2359, [https://doi.org/10.1016/0016-7037\(94\)90015-9](https://doi.org/10.1016/0016-7037(94)90015-9), 1994.
- 481 [Ballabio, C., Jiskra, M., Osterwalder, S., Borrelli, P., Montanarella, L., and Panagos, P.: A spatial assessment of mercury](#)
482 [content in the European Union topsoil, *Science of the Total Environment*, 769, 144755, <https://doi.org/10.1016/j.scitotenv.2020.144755>, 2021.](#)
- 484 [Ballabio, C., Panagos, P., Lugato, E., Huang, J. H., Orgiazzi, A., Jones, A., Fernández-Ugalde, O., Borrelli, P., and](#)
485 [Montanarella, L.: Copper distribution in European topsoils: An assessment based on LUCAS soil survey, *Science of the*](#)
486 [Total Environment, 636, 282-298, <https://doi.org/10.1016/j.scitotenv.2018.04.268>, 2018.](#)
- 487
- 488 Brady, N. C. and Weil, R. R.: *The nature and properties of soils*, Pearson Education, Boston, 1104 pp., 2016.
- 489 [Bu, J. W., Sun, Z. Y., Zhou, A. G., Xu, Y. N., Ma, R., Wei, W. H., and Liu, M.: Heavy Metals in Surface Soils in the Upper](#)
490 [Reaches of the Heihe River, Northeastern Tibetan Plateau, China, 13, <https://doi.org/10.3390/ijerph13030247>, 2016.](#)
- 491 Carter, M. R. and Stewart, B. A.: *Structure and organic matter storage in agricultural soils*, CRC Press, Boca Raton, 304 pp.,
492 1995.
- 493 [Chauhan, A., Patzner, M. S., Bhattacharyya, A., Borch, T., Fischer, S., Obst, M., Thomasarrigo, L. K., Kretzschmar, R.,](#)
494 [Mansor, M., Bryce, C., Kappler, A., and Joshi, P.: Interactions between iron and carbon in permafrost thaw ponds,](#)
495 [*Science of the Total Environment*, 946, 174321, <https://doi.org/10.1016/j.scitotenv.2024.174321>, 2024.](#)
- 496 Cheng, C. J., He, N. P., Li, M. X., Xu, L., Cai, W. X., Li, X., Zhao, W. W., Li, C., and Sun, O. J.: Plant species richness on
497 the Tibetan Plateau: patterns and determinants, *Ecography*, 2023, <https://doi.org/10.1111/ecog.06265>, 2022.
- 498 Chen, J. H., Wang, Y. F., Sun, J., Zhang, J. X., Zhang, J. T., Wang, Y. X., Zhou, T. C., Huo, H. Y., and Liang, E. Y.: Linking
499 ecosystem service benefit and grazing prohibition intensity can better optimize fence layout in northern Tibet, *Land*
500 *Degradation Development*, 34, 2038-2051, <https://doi.org/10.1002/ldr.4587>, 2023.
- 501 Dallman, P. R.: Biochemical basis for the manifestations of iron deficiency, *Annual Review of Nutrition*, 6, 13-40,
502 <https://doi.org/10.1146/annurev.nu.06.070186.000305>, 1986.
- 503 Dijkshoorn, J. A., van Engelen, V. W. P., and Huting, J. R. M.: Soil and landform properties for LADA partner countries
504 (Argentina, China, Cuba, Senegal and The Gambia, South Africa and Tunisia), ISRIC Report 2008/06 and GLADA
505 Report 2008/03, ISRIC-World Soil Information and FAO, Wageningen, 23 pp., 2008.

506 Dijkstra, J. J., Meeussen, J. C. L., and Comans, R. N. J.: Leaching of heavy metals from contaminated soils: an experimental
507 and modeling study. *Environmental Science & Technology*, 38, 4390-4395, <https://doi.org/10.1021/es049885v>, 2004.

508 Fageria, N. K., Baligar, V. C., and Clark, R. B.: Micronutrients in crop production. *Advances in Agronomy*, 77, 185-268,
509 [https://doi.org/10.1016/S0065-2113\(02\)77015-6](https://doi.org/10.1016/S0065-2113(02)77015-6), 2002.

510 Fedo, C. M., Nesbitt, H. W., and Young, G. M.: Unraveling the effects of potassium metasomatism in sedimentary rocks and
511 paleosols, with implications for paleoweathering conditions and provenance, *Geology*, 23, 921-924,
512 [https://doi.org/10.1130/0091-7613\(1995\)023<0921:UTEOPM>2.3.CO;2](https://doi.org/10.1130/0091-7613(1995)023<0921:UTEOPM>2.3.CO;2), 1995.

513 Fischer, W. W., Hemp, J., and Johnson, J. E.: Manganese and the evolution of photosynthesis, *Origins of Life and Evolution*
514 *of Biospheres*, 45, 351-357, <https://doi.org/10.1007/s11084-015-9442-5>, 2015.

515 Graham, T. W.: Trace element deficiencies in cattle, *Veterinary Clinice of North America-Food Animal Practice*, 7, 153-215,
516 [https://doi.org/10.1016/S0749-0720\(15\)30816-1](https://doi.org/10.1016/S0749-0720(15)30816-1), 1991.

517 Groemping, U.: Relative importance for linear regression in R: The package relaimpo, *Journal of Statistical Software*, 17,
518 1-27, <https://doi.org/10.18637/jss.v017.i01>, 2006.

519 Guan, Z. H., Li, X. G., and Wang, L.: Heavy metal enrichment in roadside soils in the eastern Tibetan Plateau,
520 *Environmental Science and Pollution Research*, 25, 7625-7637, <https://doi.org/10.1007/s11356-017-1094-8>, 2017.

521 Gupta, U. C., Wu, K., and Liang, S.: Micronutrients in soils, crops, and livestock. *Earth Science Frontiers*, 15, 110-125,
522 2008.

523 Hartmann, J., Moosdorf, N., Lauerwald, R., Hinderer, M., and West, A. J.: Global chemical weathering and associated
524 P-release-The role of lithology, temperature and soil properties, *Chemical Geology*, 363, 145-163,
525 <https://doi.org/10.1016/j.chemgeo.2013.10.025>, 2014.

526 Hartmann, M., and Six, J.: Soil structure and microbiome functions in agroecosystems, *Nature Reviews Earth &*
527 *Environment*, 4, 4-18, <https://doi.org/10.1038/s43017-022-00366-w>, 2023.

528 Hänsch, R., and Mendel, R. R.: Physiological functions of mineral micronutrients (Cu, Zn, Mn, Fe, Ni, Mo, B, Cl), *Current*
529 *Opinion in Plant Biology*, 12, 259-266, <https://doi.org/10.1016/j.pbi.2009.05.006>, 2009.

530 Hou, X. Y. (Ed.): *Atlas of vegetation of China (1:1,000,000)*, Science Press, Beijing, 2019.

531 Jenny, H.: *Factors of Soil Formation: A System of Quantitative Pedology*, McGraw-Hill, New York, 1941.

532 Jones, D. L., Cross, P., Withers, P. J., DeLuca, T. H., Robinson, D. A., Quilliam, R. S., Harris, I. M., Chadwick, D. R., and
533 Edwards-Jones, G.: Nutrient stripping: The global disparity between food security and soil nutrient stocks, *Journal of*
534 *Applied Ecology*, 50, 851-862, <https://doi.org/10.1111/1365-2664.12089>, 2013.

535 [Jones, G. D., Droz, B., Greve, P., Gottschalk, P., Poffet, D., McGrath, S. P., Seneviratne, S. I., Smith, P., and Winkel, L. H. E.:](#)
536 [Selenium deficiency risk predicted to increase under future climate change, Proceedings of the National Academy of](#)
537 [Sciences of the United States of America, 114, 2848-2853, <https://doi.org/10.1073/pnas.1611576114>, 2017.](#)

538 [Lemière, B.: A review of pXRF \(field portable X-ray fluorescence\) applications for applied geochemistry, Journal of](#)
539 [Geochemical Exploration, 188, 350-363, <https://doi.org/10.1016/j.gexplo.2018.02.006>, 2018.](#)

540 Lindsay, W. L.: Chemical equilibria in soils, John Wiley and Sons Ltd., New York, 449 pp., 1979.

541 Loveland, P. and Webb, J.: Is there a critical level of organic matter in the agricultural soils of temperate regions: a review,
542 [Soil Tillage Research, 70, 1–18, \[https://doi.org/10.1016/S0167-1987\\(02\\)00139-3\]\(https://doi.org/10.1016/S0167-1987\(02\)00139-3\), 2003.](#)

543 [McLennan, S. M.: Weathering and global denudation, The Journal of Geology, 101, 295-303, <https://doi.org/10.1086/648222>,](#)
544 [1993.](#)

545 [Mesquita, M. E.: Copper and zinc competitive adsorption in schistic and granitic acid soils, Agrochimica, 42, 235-245, 1998.](#)

546 [Montgomery, D. R.: Soil erosion and agricultural sustainability, Proceedings of the National Academy of Sciences of the](#)
547 [United States of America, 104, 13268-13272, <https://doi.org/10.1073/pnas.0611508104>, 2007.](#)

548 Moreno-Jimenez, E., Maestre, F. T., Flagmeier, M., Guirado, E., Berdugo, M., Bastida, F., Dacal, M., Díaz-Martínez, P.,
549 Ochoa-Hueso, R., Plaza, C, Rillig, MC., Crowther, T. W., and Delgado-Baquerizo, M.: Soils in warmer and less
550 developed countries have less micronutrients globally, [Global Change Biology, 29, 522-532,](#)
551 <https://doi.org/10.1111/gcb.16478>, 2023.

552 Moreno-Jimenez, E., Plaza, C., Saiz, H., Manzano, R., Flagmeier, M., and Maestre, F. T.: Aridity and reduced soil
553 micronutrient availability in global drylands, [Nature Sustainability, 2, 371-377,](#)
554 <https://doi.org/10.1038/s41893--019-0262-x>, 2019.

555 Mu, C. C., Zhang, F., Mu, M., Chen, X., Li, Z. L., and Zhang, T. J.: Organic carbon stabilized by iron during slump
556 deformation on the Qinghai-Tibetan Plateau, [Catena, 187, 104282, <https://doi.org/10.1016/j.catena.2019.104282>, 2020.](#)

557 Mu, C. C., Zhang, T. J., Zhao, Q., Guo, H., Zhong, W., Su, H., and Wu, Q.B.: Soil organic carbon stabilization by iron in
558 permafrost regions of the Qinghai-Tibet Plateau, [Geophysical Research Letters, 43, 10286-10294,](#)
559 <https://doi.org/10.1002/2016GL070071>, 2016.

560 Myers, S. S., Zanobetti, A., Kloog, I., Huybers, P., Leakey, A. D., Bloom, A. J., Carlisle, E., Dietterich, L. H., Fitzgerald, G.,
561 Hasegawa, T., Holbrook, N. M., Nelson, R. L., Ottman, M. J., Raboy, V., Sakai, H., Sartor, K. A., Schwartz, J.,
562 Seneweera, S., Tausz, and M., Usui, Y.: Increasing CO₂ threatens human nutrition, [Nature, 510, 139-142,](#)
563 <https://doi.org/10.1038/nature13179>, 2014.

564 Nesbitt, H.W., and Young, G.M.: Early Proterozoic climates and plate motions inferred from major element chemistry of
565 lutites, *Nature*, 299, 715-717, <https://doi.org/10.1038/299715a0>, 1982.

566 Ochoa-Hueso, R., Plaza, C., Moreno-Jimenez, E., and Delgado-Baquerizo, M.: Soil element coupling is driven by ecological
567 context and atomic mass, *Ecology Letters*, 24, 319-326, <https://doi.org/10.1111/ele.13648>, 2020.

568 O'Hara, G. W.: Nutritional constraints on root nodule bacteria affecting symbiotic nitrogen fixation: A review, *Australian*
569 *Journal of Experimental Agriculture*, 41, 417-433, <https://doi.org/10.1071/EA00087>, 2001.

570 Pachauri, R. K., Allen, M. R., Barros, V. R., Broome, J., Cramer, W., Christ, R., Church, J. A., Clarke, L., Dahe, Q., and
571 Dasgupta, P.: Climate change 2014: Synthesis report. Contribution of Working Groups I, II and III to the Fifth
572 Assessment Report of the Intergovernmental Panel on Climate Change, IPCC, Geneva, Switzerland, 151 pp., 2014.

573 Piñeiro, G., Perelman, S., Guerschman, J. P., and Paruelo, J. M.: How to evaluate models: Observed vs. predicted or
574 predicted vs. observed? *Ecological Modelling*, 216, 316-322, <https://doi.org/10.1016/j.ecolmodel.2008.05.006>, 2008.

575 Potter, C. S., Randerson, J. T., Field, C. B., Matson, P. A., Vitousek, P. M., Mooney, H. A., and Klooster, S. A.: Terrestrial
576 ecosystem production: A process model based on global satellite and surface data, *Global Biogeochemical Cycles*, 7,
577 811–841, <https://doi.org/10.1029/93GB02725>, 1993.

578 Prestele, R., Alexander, P., Rounsevell, M. D., Arneth, A., Calvin, K., Doelman, J., Eitelberg, D. A., Engström, K., Fujimori,
579 S., Hasegawa, T., Havlik, P., Humpenoeder, F., Jain, A. K., Krisztin, T., Kyle, P., Meiyappan, P., Popp, A., Sands, R. D.,
580 Schaldach, R., Schuengel, J., Stehfest, E., Tabeau, A., Van Meijl, H., Van Vliet, J., Verburg, P. H.: Hotspots of
581 uncertainty in land-use and land-cover change projections: A global-scale model comparison, *Global Change Biology*,
582 22, 3967-3983, <https://doi.org/10.1111/gcb.13337>, 2016.

583 Quesada, C. A., Lloyd, J., Schwarz, M., Patino, S., Baker, T. R., Czimczik, C., Fyllas, N. M., Martinelli, L., Nardoto, G. B.,
584 Schmerler, J., Santos, A. J. B., Hodnett, M. G., Herrera, R., Luizao, F. J., Arneth, A., Lloyd, G., Dezzio, N., Kuhlmann,
585 I., Raessler, M., Brand, W. A., Geilmann, H., Moraes Filho, J. O., Carvalho, F. P., Araujo Filho, R. N., Chaves, J. E.,
586 Cruz Junior, O. F., Pimentel, T. P., and Paiva, R.: Variations in chemical and physical properties of Amazon forest soils
587 in relation to their genesis, *Biogeosciences*, 7, 1515-1541, <https://doi.org/10.5194/bg-7-1515-2010>, 2010.

588 Schmidt, W., Thomine, S., and Buckhout, T. J.: Iron nutrition and interactions in plants, *Frontiers in Plant Science*, 10, 1670,
589 <https://doi.org/10.3389/fpls.2019.01670>, 2020.

590 Simon M. N.: *Inductively Coupled Plasma Mass Spectrometry Handbook*, Blackwell Publishing, Oxford, 2005.

591 Stefan, B., Jiménez-Vicente, E., Echavarri-Erasun, C., and Rubio, L. M.: *Biosynthesis of Nitrogenase Cofactors*, *Chemical*
592 Reviews, 120, 4919-5794, <https://doi.org/10.1021/acs.chemrev.9b00489>, 2020.

593 Stehfest, E., van Zeist, W. J., Valin, H., Havlik, P., Popp, A., Kyle, P., Tabeau, A., Mason-D'Croz, D., Hasegawa, T., Bodirsky,
594 B. L., Calvin, K., Doelman, J. C., Fujimori, S., Humpenoeder, F., Lotze-Campen, H., van Meijl, H., and Wiebe, K.: Key
595 determinants of global land-use projections, *Nature Communications*, 10, 1-10,
596 <https://doi.org/10.1038/s41467-019-09945-w>, 2019.

597 St Clair, S. B. S., and Lynch, J. P.: The opening of Pandora's Box: Climate change impacts on soil fertility and crop nutrition
598 in developing countries, *Plant and Soil*, 335, <https://doi.org/10.1007/s11104-010-0328-z101-115>, 2010.

599 [Tack, F.M., Verloo M.G.: Chemical speciation and fractionation in soil and sediment heavy metal analysis: a review,](#)
600 [International Journal of Environmental Analytical Chemistry](#) 59, 225-238. <https://doi:10.1080/03067319508041330>,
601 [1995.](#)

602 [Thauer, P. K.: Methyl \(Alkyl\)-Coenzyme M Reductases: Nickel F-430-Containing Enzymes Involved in Anaerobic Methane](#)
603 [Formation and in Anaerobic Oxidation of Methane or of Short Chain Alkanes,](#) *Biochemistry*, 58, 5198-5220.
604 <https://doi:10.1021/acs.biochem.9b00164>, 2019.

605 Trabucco, A. and Zomer, R. J.: Global Aridity Index and Potential Evapo-Transpiration (ET0) Climate Database v2, CGIAR
606 Consortium for Spatial Information (CGIAR-CSI) [data set], <https://cgiarcsi.community>, 2018.

607 [Van, Eynde, E., Fendrich, A. N., Ballabio, C., and Panagos, P.: Spatial assessment of topsoil zinc concentrations in Europe,](#)
608 [Science of the Total Environment](#), 892, 164512, <https://doi.org/10.1016/j.scitotenv.2023.164512>, 2023.

609 White, P. J., and Broadley, M. R.: Biofortifying crops with essential mineral elements. *Trends in Plant Science*, 10, 586-593,
610 <https://doi.org/10.1016/j.tplants.2005.10.001>, 2005.

611 [Yoo, K., Amundson, R., Mudd, S. M., Sanderman, J., Amundson, R., and Blum, A.: Spatial patterns and controls of soil](#)
612 [chemical weathering rates along a transient hillslope,](#) *Earth and Planetary Science Letters*, 288, 184-193,
613 <https://doi.org/10.1016/j.epsl.2009.09.021>, 2006.

614 [Zhang, H., Wang, Z. F., Zhang, Y. L., and Hu, Z. J.: The effects of the Qinghai-Tibet railway on heavy metals enrichment in](#)
615 [soils,](#) *Science of the Total Environment*, 439, 240-280, <https://doi.org/10.1016/j.scitotenv.2012.09.027>, 2012.